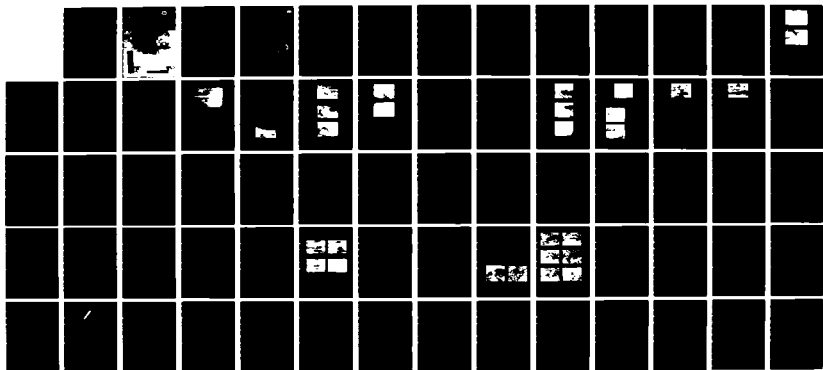HYDRAULIC MODEL STUDY OF PORT HURON ICE CONTROL
STRUCTURE(U) COLD REGIONS RESEARCH AND ENGINEERING LAB
HANOVER NH D J CALKINS ET AL. NOV 82 CRREL-82-34

F/G 8/12   NL
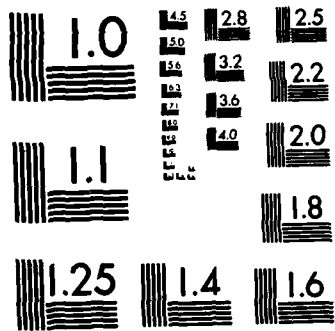
END

FILMED

DTIC

MICROCOPY RESOLUTION TEST CHART
NATIONAL BUREAU OF STANDARDS-1963-A

CRREL

REPORT 82-34

AD A123715

Hydraulic model study of Port Huron ice control structure

US Army Corps of Engineers
Cold Regions Research &
Engineering Laboratory
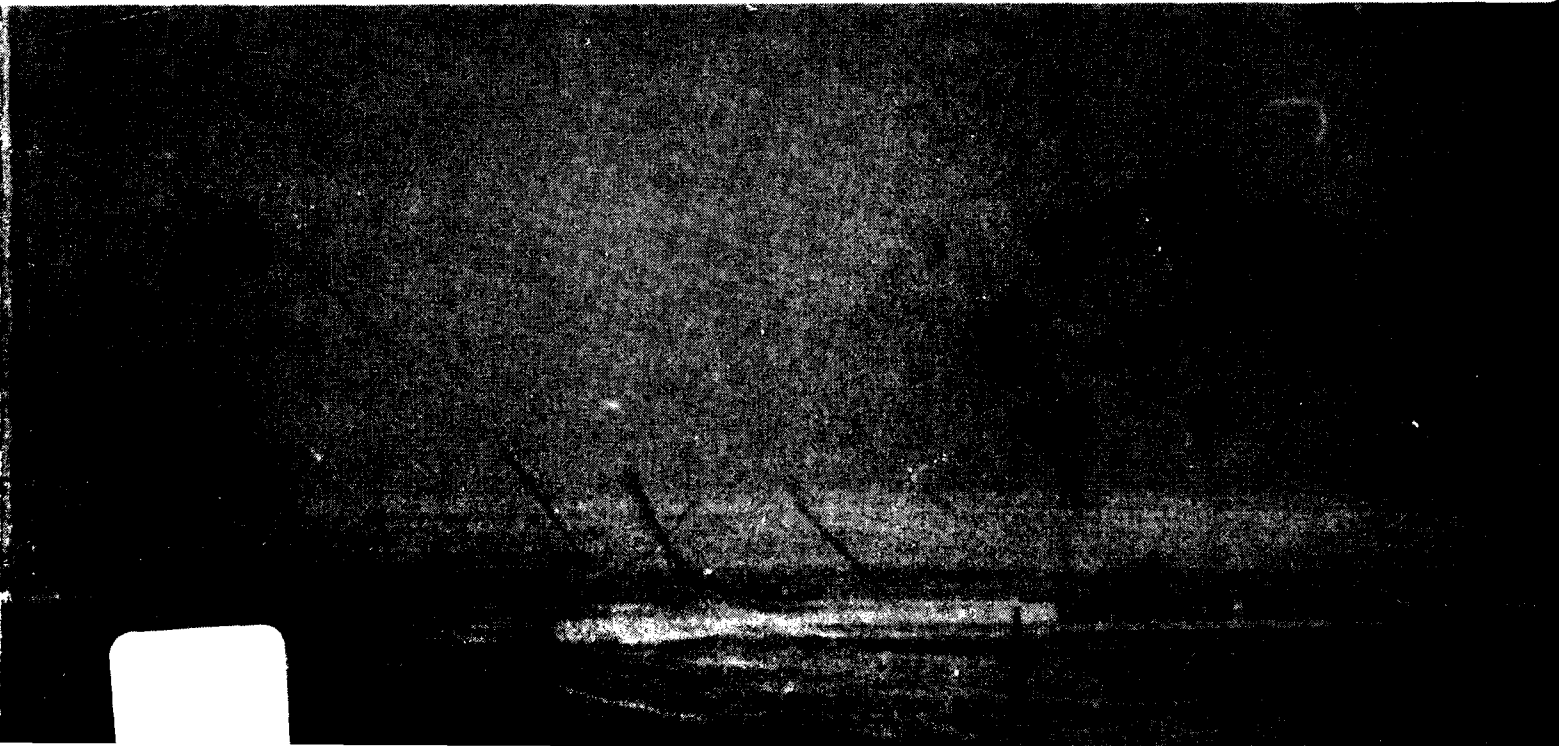
Cover: Ice arch between Port Huron, Michigan, and Sarnia, Ontario. (Photograph provided by Detroit District, Corps of Engineers.)

CRREL Report 82-34

November 1982

Hydraulic model study of Port Huron ice control structure

D.J. Calkins, D.S. Deck and D.S. Sodhi

DTIC

JAN 25 1983

H

REPORT DOCUMENTATION PAGE		READ INSTRUCTIONS BEFORE COMPLETING FORM
1. REPORT NUMBER CRREL Report 82-34	**2. GOVT ACCESSION NO.** AD - A123715	**3. RECIPIENT'S CATALOG NUMBER**
4. TITLE (and Subtitle) HYDRAULIC MODEL STUDY OF PORT HURON ICE CONTROL STRUCTURE		**5. TYPE OF REPORT & PERIOD COVERED**
		6. PERFORMING ORG. REPORT NUMBER
7. AUTHOR(s) D.J. Calkins, D.S. Deck and D.S. Sodhi		**8. CONTRACT OR GRANT NUMBER(s)**
9. PERFORMING ORGANIZATION NAME AND ADDRESS U.S. Army Cold Regions Research and Engineering Laboratory Hanover, New Hampshire 03755		**10. PROGRAM ELEMENT, PROJECT, TASK AREA & WORK UNIT NUMBERS**
11. CONTROLLING OFFICE NAME AND ADDRESS U.S. Army Engineer District, Detroit Detroit, Michigan		**12. REPORT DATE** November 1982
		13. NUMBER OF PAGES 68
14. MONITORING AGENCY NAME & ADDRESS(if different from Controlling Office)		**15. SECURITY CLASS. (of this report)** Unclassified
		15a. DECLASSIFICATION/DOWNGRADING SCHEDULE

16. DISTRIBUTION STATEMENT (of this Report)

Approved for public release; distribution unlimited.

17. DISTRIBUTION STATEMENT (of the abstract entered in Block 20, if different from Report)

18. SUPPLEMENTARY NOTES

19. KEY WORDS (Continue on reverse side if necessary and identify by block number)

Great Lakes
Hydraulic model—refrigerated
Ice control structure
Ice discharge and vessels

20. ABSTRACT (Continue on reverse side if necessary and identify by block number)

The ice discharge through an opening in an ice control structure was documented to be a function of the floe size, ice type, ice floe conditions and vessel direction. The model data for the average ice discharge per vessel transit scaled to prototype values compared favorably with data taken at the St. Marys River ice control structure (ICS). The model results of the force measurements were also consistent with data taken at the St. Marys ICS. The dynamic loading conditions were independent of vessel direction.

The dynamic loading to the structure using 3 types of ice (plastic, natural and urea-doped) showed a considerable difference in their means and standard deviations. The urea-doped ice was evaluated for dynamic loading conditions,

20. Abstract (cont'd).

and reasonable peak values of 3 to 5 times the mean load at each measuring position were recorded, independent of vessel direction.

It appears that synthetic random ice floes may be used in model studies where ice discharge through an opening in a structure needs to be documented. This study shows the synthetic random ice floe discharge to fall reasonably within the values obtained for natural ice discharge for both rafted and non-rafted ice fields above the ICS. However, the question of whether synthetic ice can be used for analyzing force distributions and dynamic force loading criteria cannot be fully answered at this time because the load distributions of the synthetic and natural floes appear to differ.

ii

PREFACE

iii

CONTENTS

ILLUSTRATIONS

TABLES

HYDRAULIC MODEL STUDY OF PORT HURON ICE CONTROL STRUCTURE

D.J. Calkins, D.S. Deck and D.S. Sodhi

INTRODUCTION

In 1978 the U.S. Army Engineer District, Detroit, requested that CRREL undertake a study to evaluate various methods for ice control at the outlet of Lake Huron because of potential problems associated with extended winter navigation in this area. Several studies were needed to properly determine the type of ice control structure (ICS), its location and design forces.

This report focuses on the results of a refrigerated hydraulic model study for determining the optimum siting of an ICS. Previous modeling studies of ice control structures with provisions for navigational openings have all been conducted in warm environments using synthetic ice (Calkins and Ashton 1975, Acres American 1975, Arctec 1978).

The Ice Engineering Facility at CRREL allows us to operate a physical model in a cold environment where natural ice can be grown for the experimental work. In addition, synthetic ice can be tested for comparison with the data from the natural ice tests. In this study, field data provided by the Detroit District from the performance of the St. Marys River ice boom (Acres American 1975) could be compared with the modeling data.

SCOPE OF WORK

The basic objective of the Lake Huron ice control study was to provide the necessary criteria for detailed design of the ice control structure at Port Huron. The two major design criteria for the ICS are 1) the configuration and 2) the forces. The configuration of the ICS will be determined by three factors: 1) orientation, 2) location and 3) size of opening. The forces on the ICS are composed of four primary components acting on the ice: 1) wind, 2) water, 3) ship-induced forces, and 4) wave forces.

The diversity of factors affecting the two design criteria was such that the research was divided into 9 studies, some requiring modeling and others not.

The following factors were modeled in the laboratory to determine their impact on the ICS: 1) ice discharge through different size openings, 2) ice forces and 3) orientation locations.

Six other studies did not require modeling: 1) estimation of ice discharge for natural conditions, 2) analysis of wind data at Port Huron, 3) evaluation of present and future ice control structures

subjected to ship passage, 4) impact of extending the ice cover on Lake Huron, 5) physical and photographic documentation of ice conditions at the site, and 6) winter measurement of flow velocity beneath the ice cover.

ICE DISCHARGE FROM LAKE HURON INTO ST. CLAIR RIVER

Figure 1 is a general location map of the major water and land masses in the area of Port Huron, Michigan. The average annual surface ice discharge (December-April) passing from Lake Huron into the St. Clair River is approximately 907 km^2 (350 mile^2) as gathered from five years of record. Since observations were made only during daylight hours, this value is twice the total of the daylight observations. The maximum and minimum annual values are 1814 km^2 (700 mile^2) and 438 km^2 (169 mile^2). The average value of the ice discharge represents less than 1.5% of the surface area of Lake Huron.

The ice discharge in terms of the percentage of surface area passing through the 305-m (1000-ft, entrance width to St. Clair River was abstracted from daylight time-lapse photography for six winter seasons, 1971-1976. The flow velocity through this 305-m section varied due to fluctuations in lake level and flow discharge, but an average of 1.45 m/s (4.75 ft/s) was used to determine the surface ice discharge. The ice thickness could not be measured from the photography; only a relative indication of thin or thick ice could be seen by observing the surface conditions of the ice floes on the photos. Figure 2 shows airphotos taken by the Detroit District at Port Huron of the ice discharge on 23 January 1973.

The data for 1975-76 contain several large time gaps due to camera malfunctions; the data for the other five years have only a few missing days and are of good quality. To distinguish between no data and zero ice discharge, a value of 2% concentration is plotted in the accompanying figures to represent zero ice discharge.

The ice concentrations were measured by projecting the time-lapse photography on a gridded screen and visually averaging the daily ice runs into six categories; 0, 0-10%, 11-25%, 26-50%, 51-75% and 76-100%.
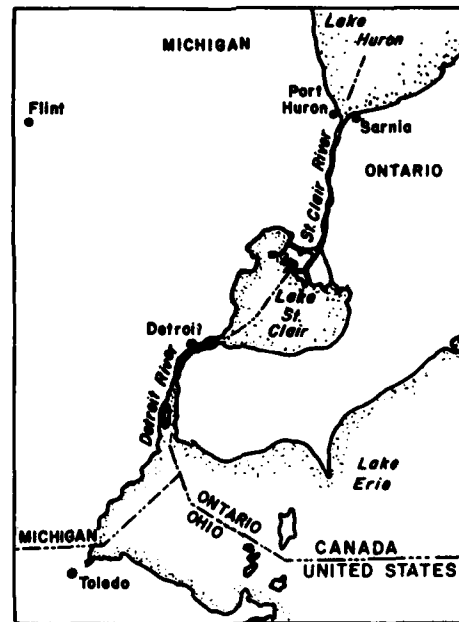
Figure 1. General location of study area.

2
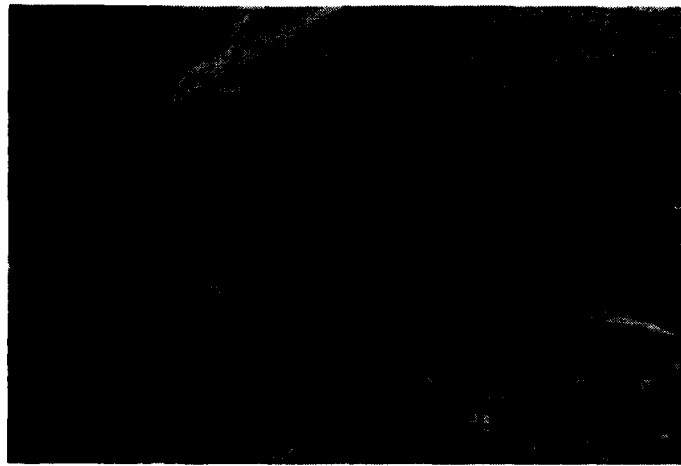
a. Ice discharge from Lake Huron into the St. Clair River.
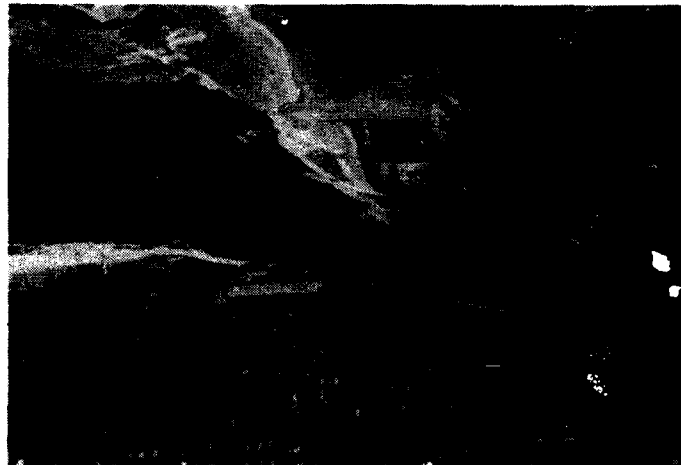
b. Same view as a except 5 min later.

Figure 2. Aerial views of ice discharge—Port Huron, 23 January 1973.

The ice discharge into the St. Clair River, in percentage concentration for the months of March 1972 and March 1974, is shown in Figures 3 and 4 to illustrate the variability from one winter season to another. The within-season variability of ice discharge can also be seen in the data for January and February 1975 in Figures 5 and 6. Due to this high variability from day to day and month to month, a seasonal distribution of ice discharge is needed, without regard to sequential events.

Figure 7 is a graphical representation for the percentage of time during the winter season that the ice discharge is greater than a certain value. Three values of ice discharge were chosen: 13, 19 and 26 km^2/day (5.0, 7.3 and 10.0 $mile^2$/day). These values represent surface ice concentrations at the entrance to the river of 35, 50 and 70%. With the exception of the 1971-72 winter season, the number of times large quantities of ice pass from Lake Huron into the St. Clair River is small, i.e. less than 1 day in 10 and more likely 1 day in 20.

Approximately 15% of the time during the winter season the ice discharge can exceed 13 km^2/day, and only 5% of the time will the ice discharge exceed 26 km^2/day, excluding the abnormal

3
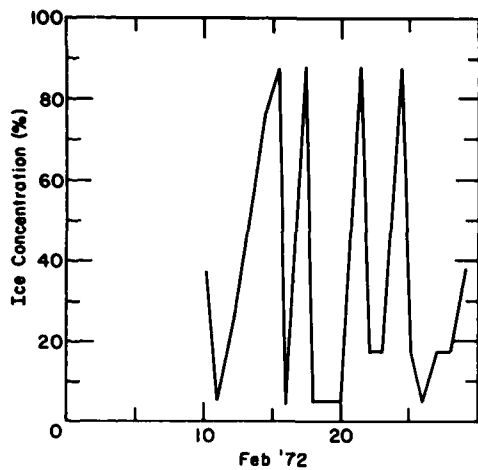
Figure 3. February 1972 ice discharge—concentration %.
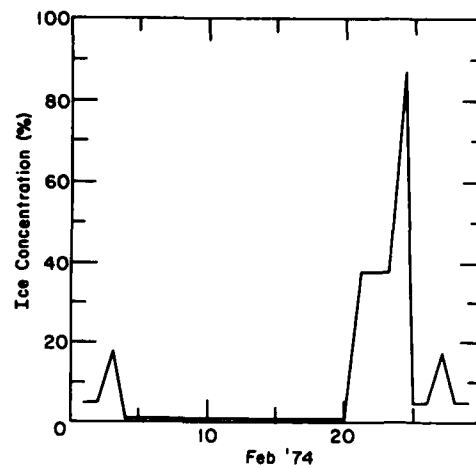
Figure 4. February 1974 ice discharge—concentration %.
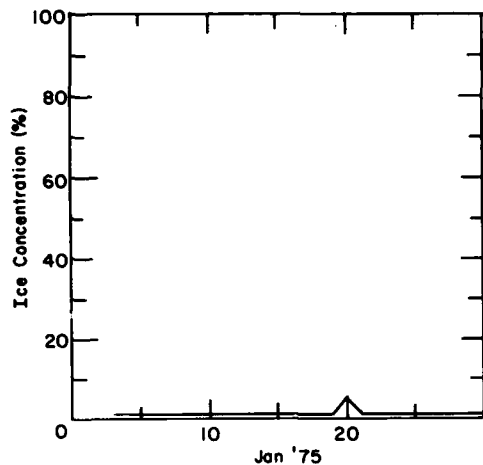
Figure 5. January 1975 ice discharge—concentration %.
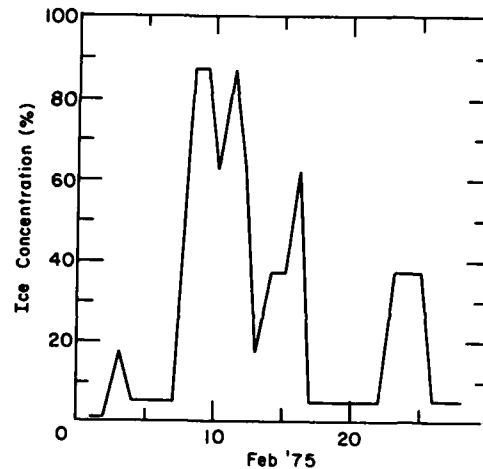
Figure 6. February 1975 ice discharge—concentration %.

season of 1971–72. During 1971–72 nearly a third of the surface ice for the entire year flowed downriver during a 9-day period in April. All other years had very minimal or no ice discharge for April.

A correlation of wind data and ice discharge at Port Huron did not offer any predictive relationship. An analysis of high ice discharge rates (11.5 km^2 or 4.4 mile^2/day) for a minimum of two consecutive days showed an average discharge value of 65 km^2 (25 mile^2) per event before the ice re-arched or the ice concentration became too low for the ice to extend upstream of Port Huron (25 events analyzed). However, the standard deviation was nearly equal to the mean ice discharge.

4
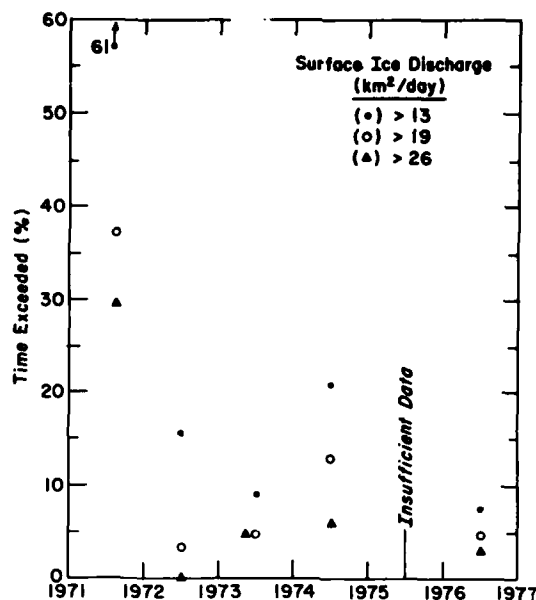
Figure 7. Percentage of time that ice discharge is exceeded on any day—Port Huron.

WATER VELOCITY PROFILES AT PORT HURON

The velocity distribution of water flow beneath an ice cover has been shown to closely follow a logarithmic distribution from the position of maximum velocity to the ice cover underside. The gradient of the velocity with depth is related to the shear stress τ_i acting on the underside of the ice cover. The velocity distribution function is

$$V_i = 2.5\, V_* \ln\left[\frac{30y}{k_i}\right] \tag{1}$$

where

V_i = velocity at any vertical position y

V_* = shear or friction velocity = $\sqrt{\tau_i/\rho_w}$

ρ_w = density of water

k_1 = equivalent sand roughness height of the ice cover underside.

Equation 2 can be integrated over the region affected by the ice cover. The lower limit is $k_i/30$, where the velocity was assumed to be zero and the upper limit is defined as Y_i, the distance to the position of maximum velocity measured from the bottom of the ice cover (see Fig. 8).

The mean velocity in the region affected by the ice cover is

$$V_{mi} = \frac{2.5\, V_*}{Y_i} \int_{k_i/30}^{Y_i} \ln\left(\frac{30}{k_i}\, y\right) dy = \frac{2.5\, V_*}{Y_i}\left[Y_i \ln\left(\frac{30}{k_i}\, Y_i\right) - Y_i + \frac{k_i}{30}\right] \tag{2}$$

which can be further simplified by neglecting the last term since it is significantly smaller than the other two terms in the bracket:

$$V_{mi} = 2.5\, V_*\left(\ln \frac{30}{k_i}\, Y_i - 1\right). \tag{3}$$

5
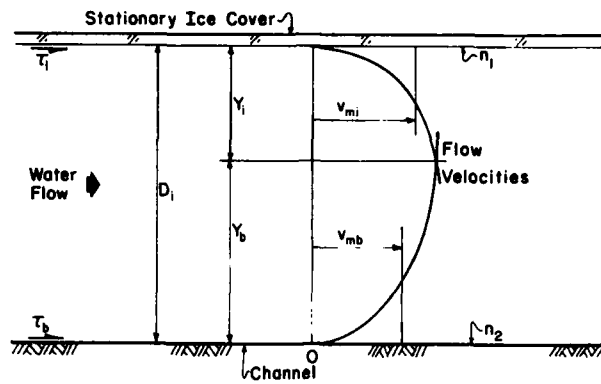
Figure 8. Velocity distribution beneath ice cover.

The equation for the maximum velocity is thus

$$V_{max} = 2.5 \, V_* \left[\ln\left(\frac{30 \, Y_{max}}{k_i}\right) - 1 \right] .$$ (4)

Substituting eq 4 into 3 yields

$$V_* = \frac{V_{max} - V_{mi}}{2.5}$$ (5)

and further reduction by the definition of the shear stress as $\rho_w \, V_*^2$ yields

$$\tau_i = \rho_w \left(\frac{V_{max} - V_{mi}}{2.5}\right)^2 .$$ (6)

Likewise the Darcy friction factor f is

$$f = \frac{8\tau_i}{\rho V_{mi}^2} = 1.28 \left(\frac{V_{max}}{V_{mi}} - 1\right)^2 .$$ (7)

The velocity distribution beneath the ice cover at Port Huron was measured at 10 locations corresponding to previously monitored sites during open water conditions. Table 1 gives a summary of the velocity distribution data below the ice.

Table 1. Summary of velocity profiles on Lake Huron, 7 February 1979.

Site	Mean vel. (m/s)	Max vel. (m/s)	Depth at max vel. (m)	Ratio Y_i/D_i	Friction velocity (m/s)	Stress (N/m²)	Friction coeff, f	Ice thick (m)
36	0.35	0.44	4.65	0.47	0.036	1.27	0.084	0.22
51	0.27	0.42	5.15	0.63	0.001	3.69	0.411	0.24
49	0.28	0.35	5.58	0.78	0.028	0.81	0.083	0.22
63	0.28	0.36	5.15	0.78	0.034	1.16	0.122	0.24
32	0.48	0.60	4.55	0.41	0.048	2.34	0.081	0.24
55	0.45	0.58	4.55	0.42	0.051	2.54	0.099	0.24
30	0.37	0.46	4.50	0.69	0.037	1.38	0.082	0.29
57	0.30	0.40	5.62	0.88	0.039	1.53	0.134	0.17
61	0.37	0.45	4.12	0.56	0.031	0.97	0.056	0.26
67	0.36	0.40	4.59	0.75	0.016	0.24	0.015	0.20
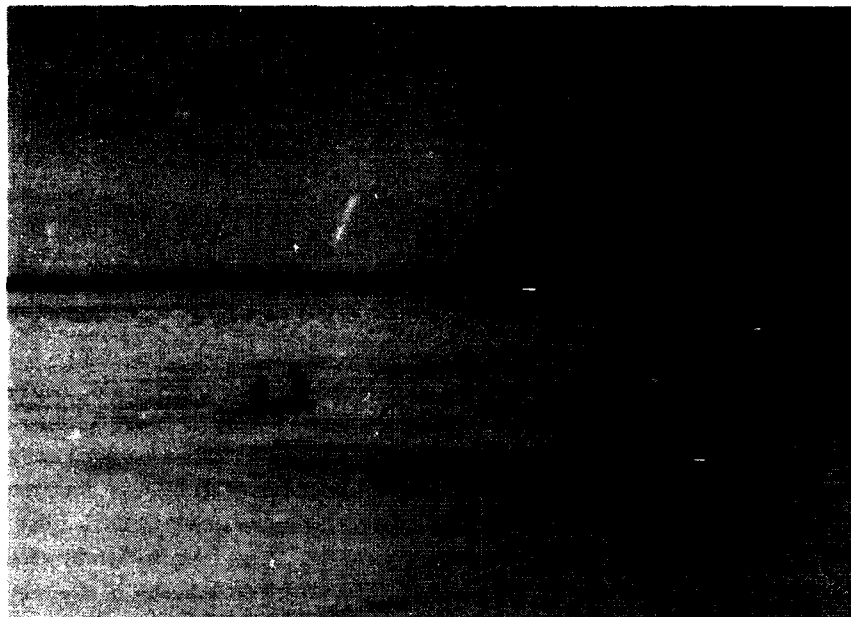
Figure 9. Measurements on the ice—Port Huron.

The basic data from Table 1 relevant to this study are the shear stress values of the ice underside. The mean value is 1.59 N/m^2 (0.034 lbf/ft^2), with a standard deviation of 1.0 N/m^2 (0.021 lbf/ft^2). By eliminating the highest and lowest value, $\tau_i = 1.5 \pm 0.63$ N/m^2. Other useful coefficients were also calculated such as V_* and k_i.

The collection of the field data was a time-consuming and slightly dangerous effort. On only one day in 15 during three separate missions to Port Huron were we successful in making the necessary measurements. This was accomplished by airlifting the people, velocity probe, ice auger, safety gear and life raft onto the ice with helicopters (see Fig. 9). The helicopter support was provided by the U.S. Coast Guard Air Station at Detroit. Triangulation data for the velocity measurement sites were radioed to the pilots by field personnel from the Detroit District, Corps of Engineers, Hydraulics and Hydrology Section, who set up on the horizontal control points.

A two-directional magnetic flow meter was used to gather the data. The probe is a 3.75-cm-diam. sphere with a resolution to 2 cm/s and a measuring volume of 1.5 sphere diameters. Velocity measurements were attempted for the full depth, but the drag on the extension rods was so great in some locations that the vibrations in the rods were excessive. After bending a few rods, only velocity measurements to the depth of maximum velocity were made.

ICE CONDITIONS

The mean air temperature data for the Port Huron area were abstracted from the Great Lakes ice cover atlas distributed by the National Oceanographic and Atmospheric Administration (Table 2). The site of the air temperature measurements was Alpena, Michigan.

The following table summarizes these monthly values in terms of degree days. The solid ice sheet thickness for a single layer can be calculated by assuming a freezeover date of 1 January by using

$$t = \alpha \sqrt{\Sigma (^\circ \text{days})} \ . \tag{8}$$

7

Table 2. Average air temperature and estimated ice thickness for
Lake Huron, Alpena, Michigan, data.

	Freezing degree days		Cumulative		Ice thickness	
	°C Days	°F Days	Σ (°C Day)	Σ (°F Day)	(m)	(ft)
Jan	277	500	277	500	0.40	1.3
Feb	223	400	500	900	0.53	1.75
Mar	83	150	583	1050	0.58	1.9
April	-83	-150	500	900	0.53	1.75

The coefficient α must account for the local geographic setting, snow cover, wind, thermal and other meteorological conditions. Using a value of approximately 0.0238 m day$^{-\frac{1}{2}}$ °C$^{-\frac{1}{2}}$ (0.7 in. day$^{-\frac{1}{2}}$ °F$^{-\frac{1}{2}}$), the maximum thickness is roughly 0.58 m (1.9 ft). The ice thickness on Lake Huron can be highly variable due to rafting and ridging, with thicknesses of 1 m (3 ft) or more common. The ice thickness distribution near the shipping track can also be highly variable and thicker due to the constant breaking of ice and deposition at the sides of the track. Large floes broken by vessel transits were observed to be deposited in layers of 3 to 4 floes thick on each side of the shipping track near Port Huron.

Airphotos are usually very descriptive in their presentation of the ice conditions at a particular location. Figures 10a-f include photography taken during typical ice conditions at Port Huron. Figures 10a-c, looking uplake, show the ice arched from shore to shore with open water extending only a few hundred to a few thousand meters above the Blue Water International Bridge. The open water areas are difficult, if not impossible, to predict, depending on ice conditions, wind, and ship traffic. A vessel track can be seen in the upper portion of the solid ice, extending into the lake.

The ice conditions at Port Huron range from the presence of only small ice floes at freezeup, to the solid cover or individual large floes during the middle of the winter, to the total breakup of ice in the spring. The ice along both shorelines can be very thick due to the pileup conditions from high winds as well as from the forces in the sustained ice arching that develops. The thickness can be as much as 6 to 7 m (20 ft) depending on the specific location. An airborne radar system was employed to measure the ice thickness distribution in the lake, but the data have not been fully

a.

Figure 10a-f. Various views of the stable ice arch between
the shore of Port Huron, Michigan, and Sarnia, Ontario,
taken during 1971-1978.

8
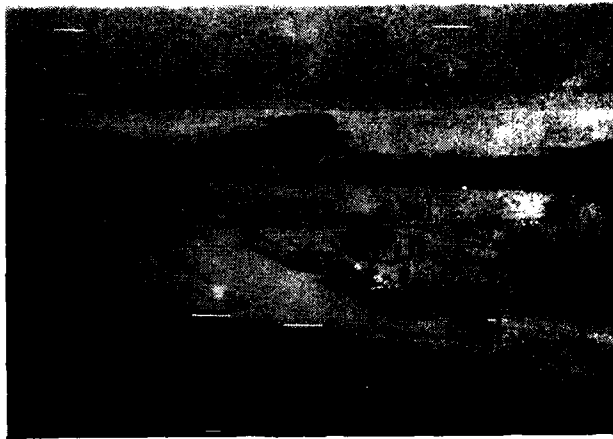
b.
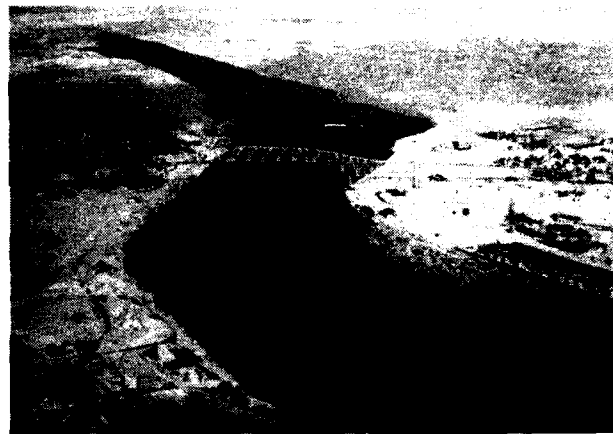
c.

d.

Figure 10a–f (cont'd).

9

e.

f.

*Figure 10a-f (cont'd). Various views of the stable ice
arch between the shore of Port Huron, Michigan, and
Sarnia, Ontario, taken during 1971-1978.*

reduced or interpreted at this time. The ground truth observations taken during these radar flights
show ice thicknesses ranging from 0.15 m to over 1 m. The large thicknesses were the result of
rafting and piling of ice floes, leading to ice covers of one to four floes in thickness.

The shore ice ridges were at least 3 m (10 ft) high in some locations during 1979 and residents
in the area talked of ridges 6 to 9 m (20 to 30 ft) high. Apparently more historical studies or
future observations are needed on shore ice pileup and its potential effects on the shoreline's en-
vironment.

PHYSICAL MODEL

Basis for selection

A physical model of the site was needed to document the following parameters: 1) ice dis-
charge through an opening in the ICS during ship transits, 2) water drag on the ice due to the ICS,

10

3) ship-induced forces on the ICS and 4) velocity patterns if permanent structures are planned. The scale of the Froude model chosen was 1:85 for both horizontal and vertical dimensions.

The model scale selection was primarily based on the Reynolds number being greater than 1000 for ice-covered conditions at a water temperature of 0°C in and near the navigational channel. This particular scale of 1:85 also allowed for sufficient surface area upstream of any proposed structure for vessel transit through the model structure. The Reynolds number criterion is thus

$$N_r = \frac{VD_i}{v} = 2000 \tag{6}$$

where V = mean velocity over the depth D_i
   D_i = depth of water from ice underside to the bed
   v = kinematic viscosity of water.

The Reynolds number of 2000 accounts for the floating ice cover changing the hydraulic radius or hydraulic mean depth R_h to approximately $D_i/2$. The kinematic viscosity of water near 0°C is nearly 1.83 times the value for water at 20°C.

To operate the hydraulic model at $T = 20°C$, the open water Reynolds number must be at least 2500 to 3000. This will ensure that the model can also be operated at $T = 0°C$ with an ice cover.

A Froude model governs when the predominant driving force is gravity, open channel flow. Principles of open channel flow can be applied to a floating ice sheet by adjusting the cross-sectional area, hydraulic radius and roughness coefficient. Since the Froude model has ensured dynamic similarity, kinematic and geometric similarity are implied. The relationship is simply

$$N_{fm}/N_{fp} = \frac{V_m/V_p}{|(g_m/g_p)(h_m/h_p)|^{1/2}} = 1 \tag{9}$$

where N_f = Froude number
   V = mean velocity vector
   h = characteristic length, taken as the depth
   g = acceleration of gravity
   m,p = model and prototype conditions respectively.

Without geometric distortion there are no differing scale factors for time, acceleration, etc., within the vertical and horizontal directions. The scaling laws for the various items such as the geometrics, mass flow, pressure, etc., can all be calculated very easily.

The more commonly used scaling factors in this report are given in Table 3 where the subscripts m and p are previously defined and r refers to their ratio.

Description

The undistorted scale of 1:85 for the fixed-bed Froude model provided accurate reproduction of the hydraulic conditions, flow velocity and direction. The model simulated an area extending from Lake Huron's entrance to the St. Clair River (Fig. 11), approximately 1.6 km (1 mi) uplake.

The hydrographic survey was supplied by the Detroit District. Template cross sections normal to the flow were established

Table 3. Scaling conversions.

	Ratio	Factor	
Length	L_p/L_m	85	L_r
Area	L_p^2/L_m^2	7225	$(L_r)^2$
Volume	L_p^3/L_m^3	6.14×10^5	$(L_r)^3$
Time	θ_p/θ_m	9.219	$(L_r)^{1/2}$
Density	ρ_p/ρ_m	1	1
Water velocity	V_p/V_m	9.219	$(L_r)^{1/2}$
Water discharge	Q_p/Q_m	6.66×10^4	$(L_r)^{5/2}$
Fluid shear stress	τ_p/τ_m	85	L_r
Forces	F_p/F_m	6.14×10^5	$(L_r)^3$

11
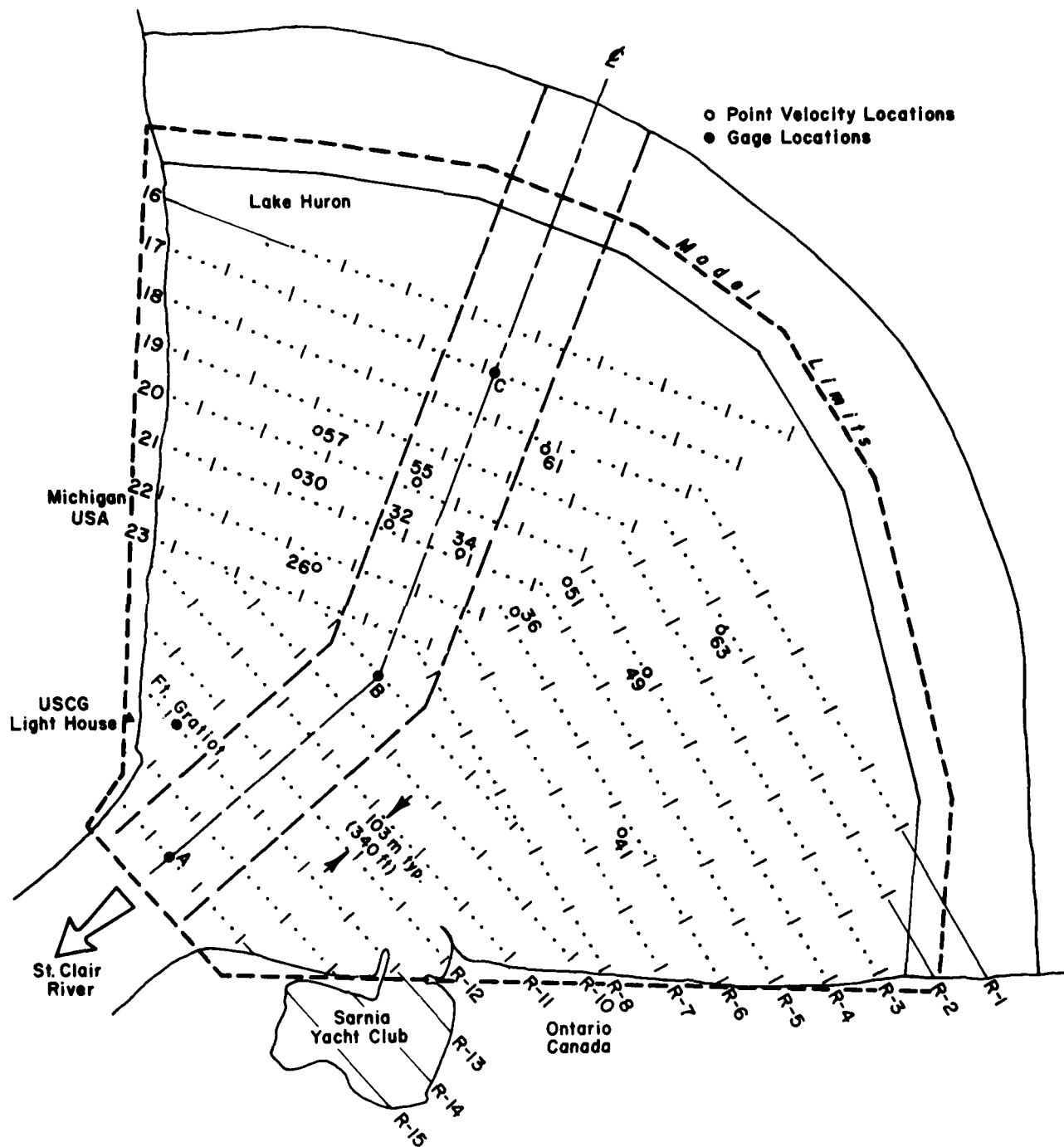
Figure 11. Model limits, measuring positions

12

a. Initial layout of model templates.
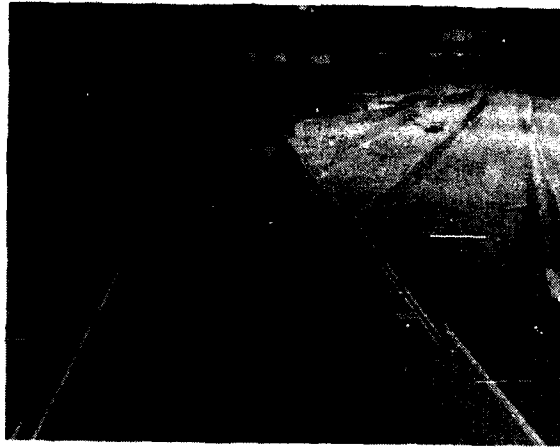
b. Partial completion of sand base for the model.

c. Nearly completed template and base foundation of sand.

Figure 12. Typical scenes during model construction.
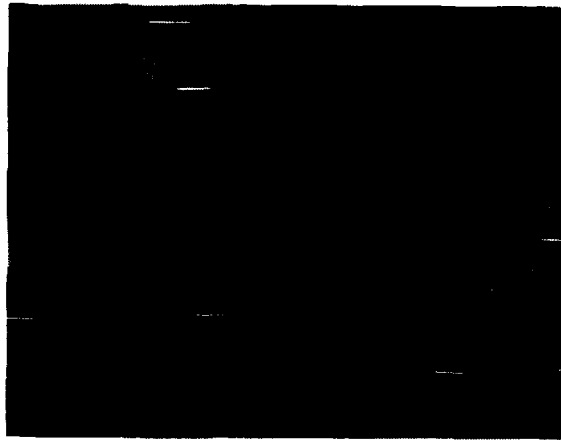
d. Placement of 5 cm (2 in.) of mortar to complete the model bed.

Figure 12 (cont'd). Typical scenes during model construction.

a. Steel reinforcement mesh placed into the mortar shell.

b. Alternate drying and curing of mortar.

Figure 13. Final phases of model construction.
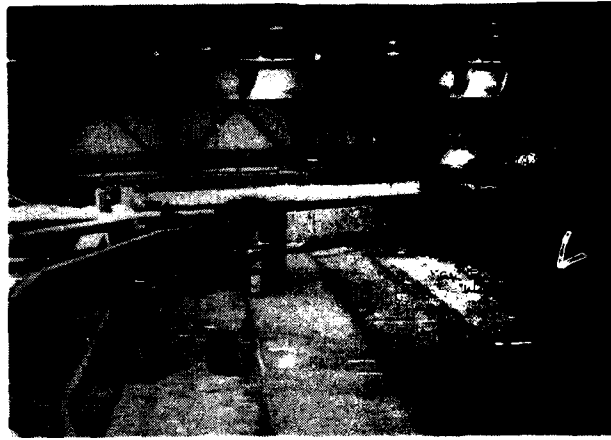
c. View of personnel coating the model with fiberglass resin.

Figure 13 (cont'd).

every 103 m (340 ft) to provide accurate bed reproduction. Figures 12a–d show typical scenes during the model construction phase. In addition to the usual sand fill–mortar skin construction for the model, other measures were taken to protect the model from alternative freeze-thaw cycles required in the testing program. The mortar was reinforced with a 10-gauge wire mesh and the entire surface was sealed with a resin over a fiberglass mat (Fig. 13a–c). These additional methods prevented significant thermal cracks and minimized the migration of moisture through the mortar skin and subbase.

Pumps supplying 0 to 0.03 m³/s (500 gpm) and 0 to 0.06 m³/s (1000 gpm) fed the 33-m- (110-ft-) long inlet trough equipped with a partitioned weir for flow control. Each pump line contained a magnetic flow meter for discharge monitoring. The downstream flow control consisted of a 3.58-m- (11.75-ft-) long flapper gate located at the end of the model area.

The water levels were measured at four locations in the model, with the Ft. Gratiot gauge (Fig. 11) used as the control gauge for the study. The other water level measurements were conducted in the center of model along an approximate stream line which coincided reasonably well with the navigation channel (see Fig. 11). These midchannel water level measurements were performed from an overhead carriage.

Instrumentation

The major instrumentation procedures consisted of calibrating 11 strain-gauged aluminum circular bars in the two horizontal directions and writing the computer programs to collect the data on the forces transmitted to these bars. The cross sensitivity between gauges for each bar was calculated and the stored data on the force levels reflected this correction for the cross sensitivity. The sensitivity of the bars for recording small deflections was limited to a 0.01-N (0.0022-lbf) change in force. The stability of the electronic data collection system (a Neff 300 controlled by a Hewlett-Packard 9845 computer) was excellent; 0.05 N (0.011 lbf) was the maximum drift over a three- to four-hour period for any one bar direction, and usually the drift less than 0.02 N.

The floating ICS was attached to the 11 vertically mounted instrumented bars, which measured the load in the two horizontal directions. These bars were attached to a square tubing frame that was in turn supported by four vertical supports (Fig. 14). The four vertical supports were located downstream of the ICS and did not interfere with the force measurements or movement of ice through the gap opening.

Figure 14. Typical view looking west of the model ship in a plastic, randomly shaped, fragmented ice field.

Model ice control structure

At the beginning of the study the type of ice control structure that would be acceptable to the surrounding environment was not known. To construct a model ICS structure at a scale of 1:85 and maintain the exact geometric replications was not practical. Since no particular ICS was being tested a compromise on the model structure to be placed was made.

A series of floating polyethylene blocks 2.5 cm x 7.5 cm x 1.25 cm thick (1 x 3 x 0.5 in.) tied together with nylon line were held in place by vertical rods. This floating ICS held the ice sheet in place and transmitted the loads to the vertical rods. By moving a frame system from which the vertical rods were suspended, the ICS could be moved in the model. The ICS was divided into two sections, each beginning at the U.S. and Canadian shorelines and extending toward the navigation channel. Adjustments in the support frame allowed for different gap openings to be studied in the ICS.

Mean velocity data of the flow beneath the ice cover at selected locations were collected using a 0.95-cm- (38-in.-) diameter two-directional magnetic flow velocity probe. Reliable documentation of the vertical velocity profile could not be measured in the model with this probe because it was too large in comparison to the water depths of 6 to 12 cm (3 to 5 in.) in the model. Therefore, velocity measurements were made only to estimate the mean velocity. Accuracy is ± 1.0 cm/s in the model.

Open water calibration

The model was adjusted to simulate conditions determined from prototype drogue studies that were conducted in May and October 1978 by the Detroit District (Fig. 15). Cylindrical 2-cm- (3/4-in.-) diam. PVC floats were used to measure the streamlines and velocities. The floats were adjusted to the proper corresponding prototype depths of measurement.

The various partitions of the inlet weir were adjusted until the flow lines in the model were in satisfactory agreement with the prototype velocities, both in magnitude and direction. The open water calibration was performed in conjunction with personnel from the Hydraulics Division of the U.S. Army Waterways Experiment Station, Vicksburg, Mississippi.

The flow used for model calibration (Fig. 15) was a result of the two drogue studies. As both flows were within 2% of each other, a flow of 5700 m³/s (201,000 cfs) with a Ft. Gratiot level of 578.87 ft was used. Although the flow lines in the model did not change appreciably for different model flows, a set of drogue data at a lower flow should have been gathered to verify the model results. Flows at different gauge elevations did not significantly change their velocity patterns or magnitudes by more than 10% over the entire model.
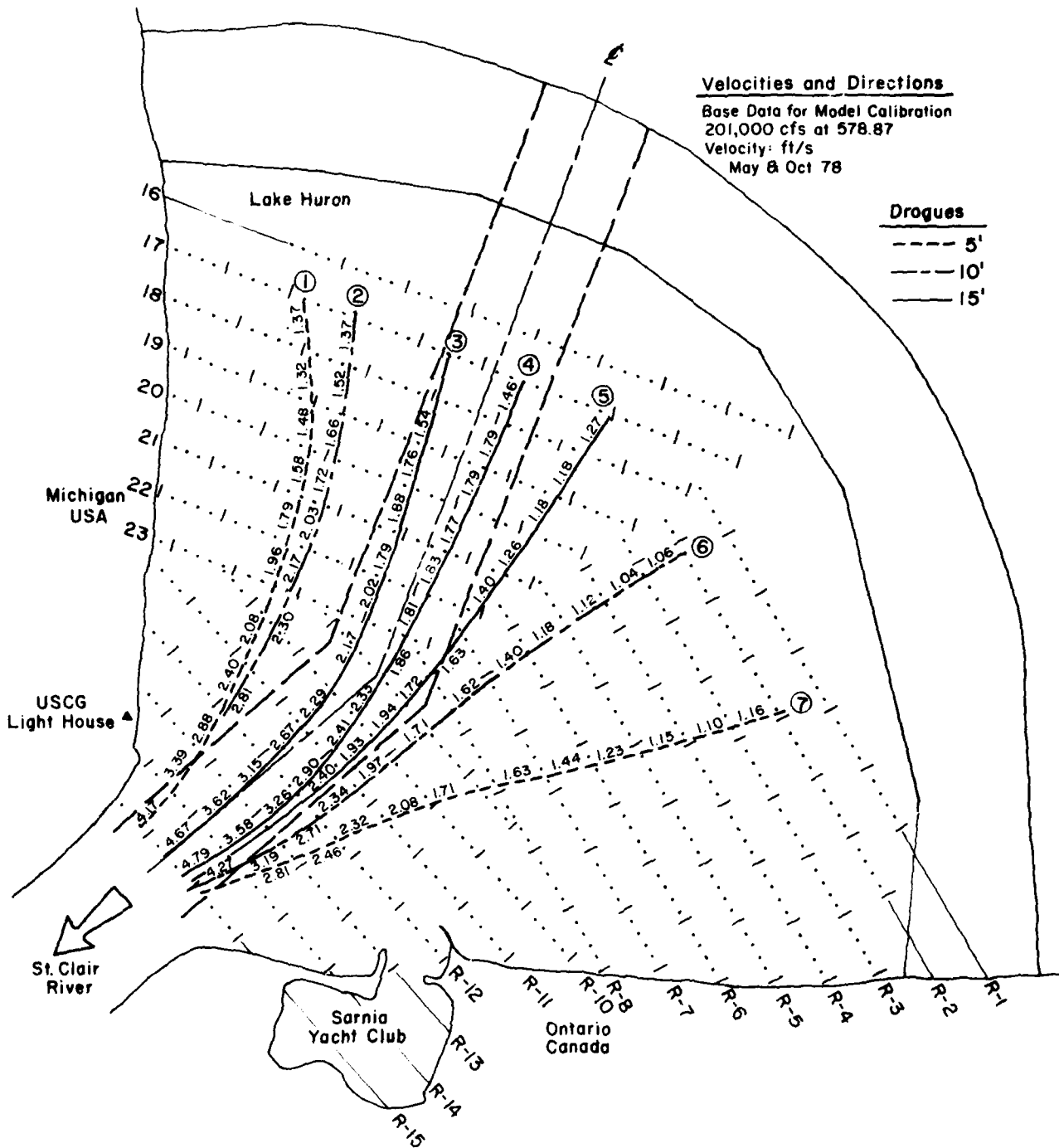
Figure 15. Baseline data for model calibration.

17

Open water tests

The mean annual winter flow (December–April) into the St. Clair River was calculated to be 4704 m³/s (166,000 ft³/s) with a standard deviation of 708 m³/s (25,000 ft³/s). After consultation with the Detroit District, three flows were evaluated: 4700 m³/s (166,000 cfs), 5385 m³/s (190,000 cfs), and 5950 m³/s (210,000 cfs) in the model. The largest flow represents approximately the maximum monthly flow recorded during the last 20 years for the winter months. The corresponding water surface elevations at the new Fort Gratiot gauge for these three flows are 175.62 m (576.19 ft), 176.22 m (578.16 ft) and 176.73 (579.8 ft), International Great Lakes Datum (IGID). The water level elevations for the same flow will vary considerably from year to year, and a 0.7-m (2.3-ft) difference in height was noticed for the mean winter flow.

The mean velocities from the model drogue study over the entire model for the three flows mentioned earlier are given in Figures 16–18. The general streamline patterns are the same and the velocities do not differ significantly in the center of the model, i.e. the navigational channel. A significant change in the flow velocities occurs along the U.S. shore due to the shallow depths extending into the lake about 100 to 200 m (328 to 656 ft).

Experimental procedures and techniques

Both plastic ice floes and natural ice grown under the refrigerated conditions in the testing area were used in the experiment. The testing techniques for the laboratory-grown ice were different from those used for the plastic ice.

The ice discharge was measured by two methods. If plastic ice were being used, then one merely had to count the number of floes passing through the opening. The tests with the plastic ice used either square floes of uniform size or randomly shaped floes whose average size was measured previously from the sample population. In this manner the area per floe was known and multiplication by the number of floes released gave the area of ice discharged. The thickness of the plastic "ice" was 0.635 cm (1/4 in.) or 0.54 m (1.77 ft) for the prototype.

The measurement of the laboratory-grown ice discharge was accomplished by weighing the amount of ice, determining the average floe thickness and counting the number of floes. From the weight measurement and ice thickness, the surface area would be computed. The average floe size was calculated by counting the number of floes per disturbance and dividing the total surface area by the number of floes. The data from several disturbances (200–500 total floes) would be used to calculate the mean floe size. These relationships are

$$A_r = \frac{W_i}{\rho_i t_i} \tag{10}$$

$$a = [A_r/N_i]^{\frac{1}{2}} \tag{11}$$

where A_r = area of ice released
W_i = mass of ice released
ρ_i = density of ice = 0.92
t_i = thickness of ice
N_i = number of ice blocks released
a = average floe size.

Flow establishment

Once the flow distribution was set with the partitioned weirs, no changes were introduced at the upstream end. The water level at the downstream portion of the model was then controlled by a gate to achieve the appropriate prototype values at the Fort Gratiot gauge.
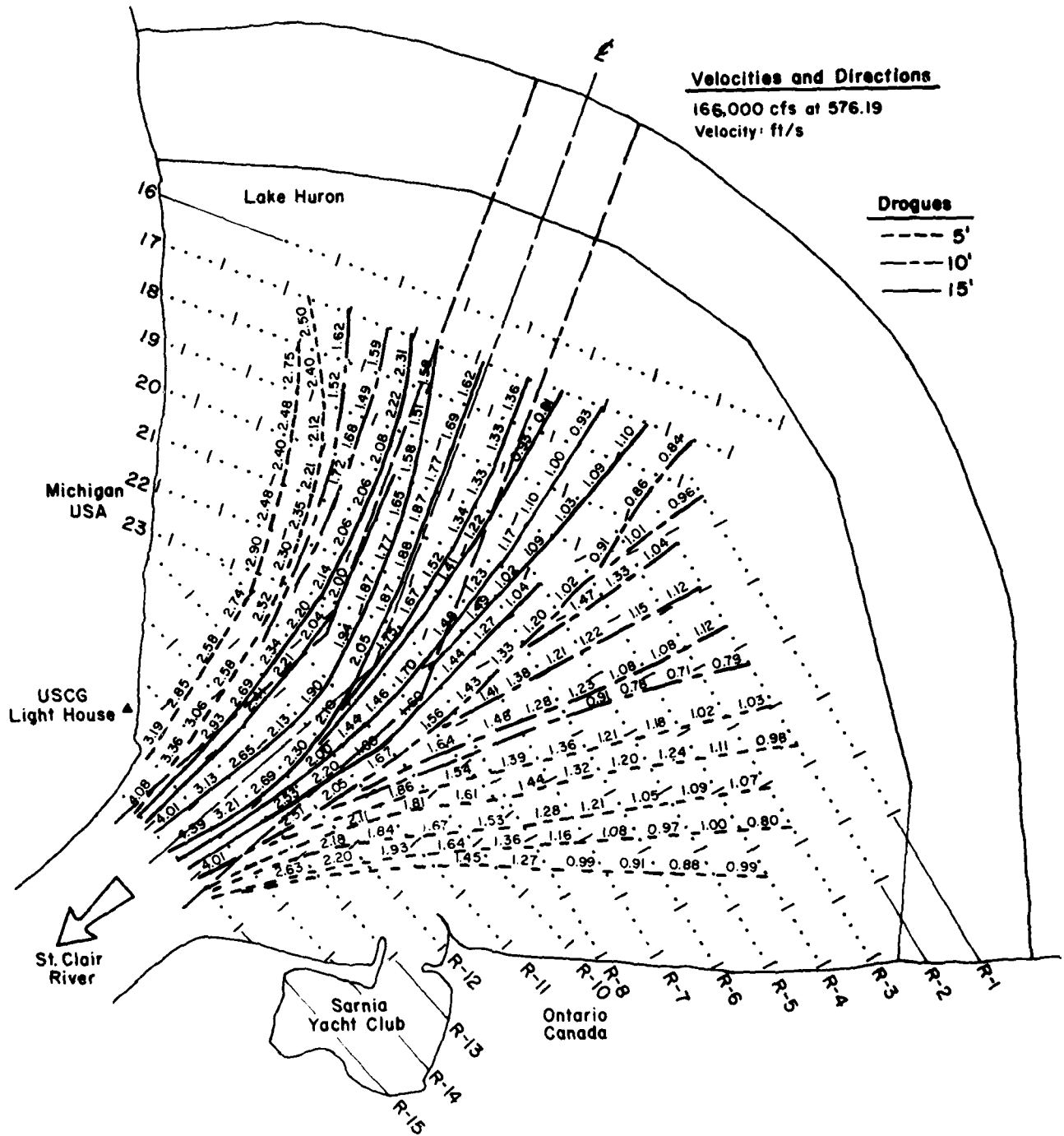
Figure 16. *Mean velocities for 4700 m³/s—drogue method.*
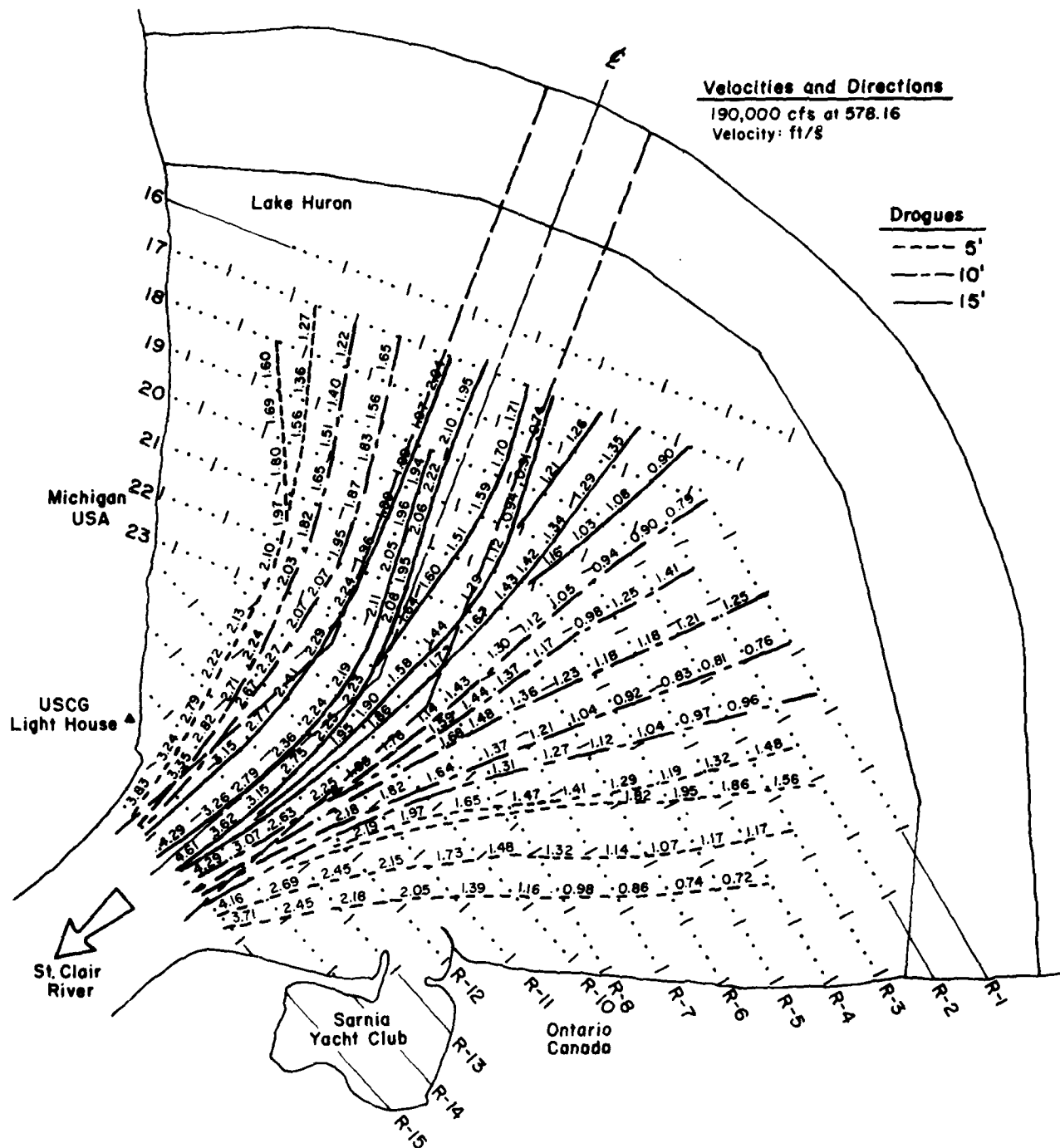
Figure 17. Mean velocities for 5385 m³/s—drogue method.
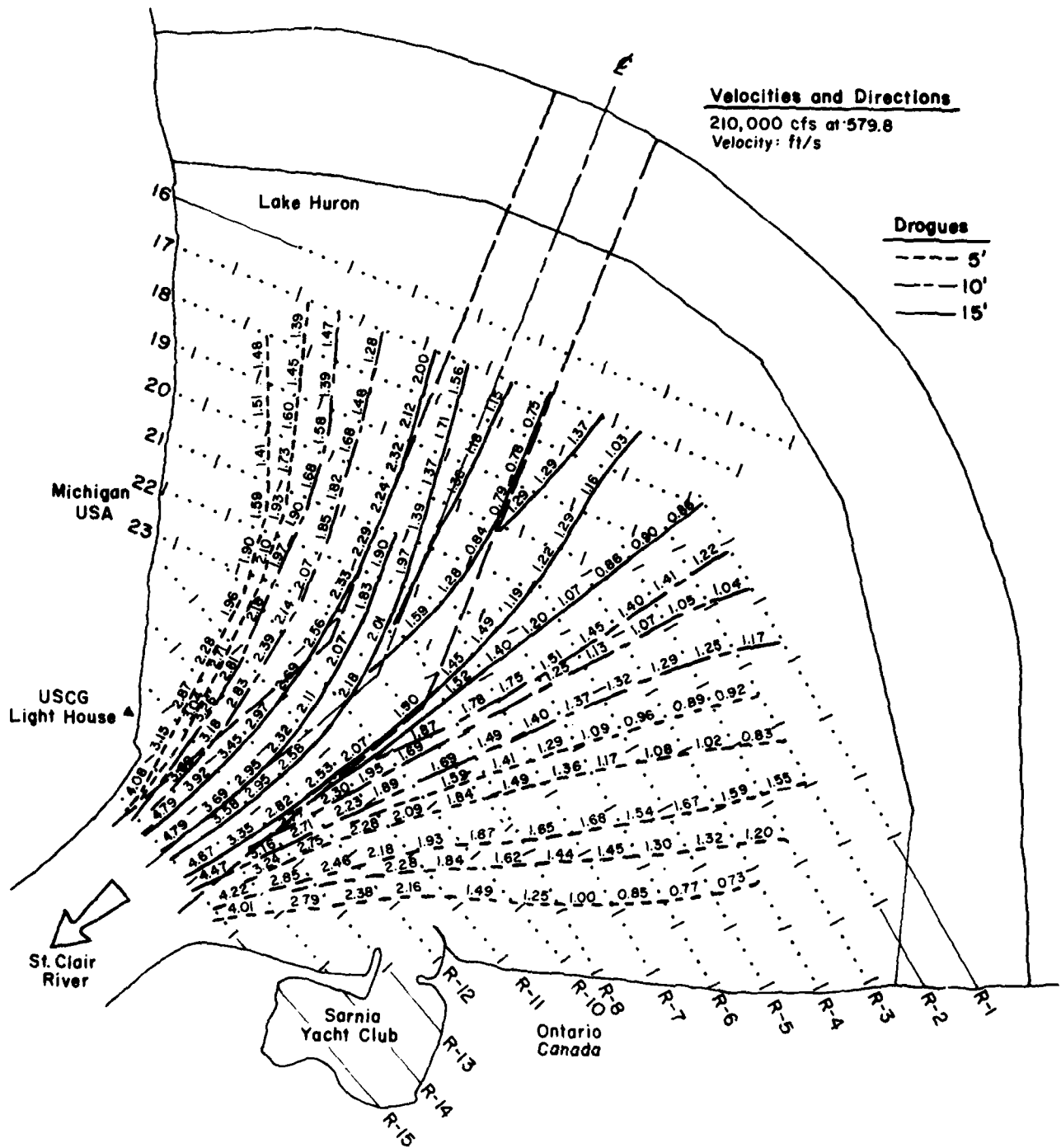
Figure 18. Mean velocities for 5950 m³/s—drogue method.

The water surface slope from points B to C (see Fig. 11) was measured for many of the tests using both plastic and natural ice, and little difference in slope was detected. In fact, measurement error was more of a problem, as the slopes were very mild (5×10^{-5}) with a vertical drop of only 0.4 mm over a distance of 8.534 m (28.0 ft). The accuracy of the point gauges was only 0.1 mm.

Artificial ice

The placement of the plastic "ice" on the water surface was done manually. The water flow in the model was reduced, and then the flow was gradually increased to the desired conditions. All experiments were started with the single layer ice floes. A small wooden stick was placed across the opening between the two ice control structures to prohibit any ice discharge until the flow conditions and water elevations were established correctly.

Natural ice

The procedure used to break the freshwater ice was again manual. The water flow was either reduced to 0.006 m³/s (100 gpm) or completely stopped, and the desired ice thickness was achieved by cooling the room overnight at the appropriate temperatures. Maintaining a small flow minimized the ice buildup in the inlet troughs and on the outlet gate and produced only a small zone in the model where the ice thickness was not uniform. Otherwise the thickness over the entire ice sheet was constant within ± 1 mm.

The ice was first broken away from the shorelines, the inlet trough and the gate so that the ice cover would float when the water discharge and levels were increased. With sufficient flow beneath the ice cover, all ice downstream of the ICS was broken up and allowed to float over the gate. During this time the room was being warmed to an air temperature slightly above freezing, which was necessary to prevent refreezing of the individual ice floes broken upstream of the ICS.

Since the study did not concern itself with modeling the breaking of a solid ice sheet by a ship, the freshwater ice was not modeled for its flexural strength. When the room air temperature was above freezing, the water discharge was stopped and the ice floes were broken into randomly shaped pieces by walking carefully over the ice, and further breaking them into the desired flow size with blunt wooden probes. The smallest average floe size for any test was 10 cm (model size). When the ice breaking was completed, the initial readings for the force measurements would be taken and then the water flow would be increased to the proper conditions. The purpose of decreasing the flow was to minimize the layering of the ice floes during breakage. As with the plastic floes, a single layer of fragmented ice was the starting point for all tests.

The model ship was loaned to CRREL by the Department of Marine Architecture, University of Michigan. Its scaled-up prototype dimensions are 310 m (1020 ft) in length with a beam of 29 m (95 ft) and a draft of 8.23 m (27 ft). The ship was guided by a pulley system and driven by a variable speed motor. To eliminate the problem of turning the ship around after every transit, the stern section was replaced by an identical bow shape. This allowed us to run alternate vessel passages up and down through the ice control structure and ice field with minimal delay and without disturbing the ice field.

A typical test procedure would generally follow the guidelines below:
1. Select ICS orientation, gap opening and establish a low flow.
2. Grow ice sheet or place plastic "ice" on water surface.
3. Eliminate all ice downstream of ICS.
4. Break ice into desired flow size.
5. Take initial force reading on ICS at very low or no flow.
6. Adjust flow and water level at Ft. Gratiot to desired conditions.
7. Transit vessel uplake through ICS opening.
8. Measure ice discharge.
9. Take force measurements after ice has stopped moving.
10. Transit vessel downlake through ICS opening.
11. Measure ice discharge.

22

12. Take force measurements after ice has stopped moving.

13. Repeat steps 7 through 12 until ice field is depleted.

If dynamic force measurements were being taken, a continuous measurement of the load on all 11 bars was monitored during the ship transit through the gap opening. The scan rate was 3 samples/second for 22 channels of force data, i.e. 11 bar positions measuring forces in both x and y directions.

Ice cover calibration

The calibration of the model for ice-covered conditions was verified by setting the model's Ft. Gratiot gauge at the desired winter level and then determining if a properly scaled water shear stress was achieved. The prototype shear stresses calculated from velocity profiles beneath the ice cover are given in Table 1. The average of eight measurements, excluding the highest and lowest readings, was 1.5 N/m² (0.03 lbf/ft²), s.d. = 0.63 N/m² (0.14 lbf/ft²) with a range of 0.81 to 2.54 N/m².

The shear stresses of the water against the ice cover in the model were calculated directly by isolating the ice cover from the shoreline, determining the load to the ice control structure from the instrumented bars, and dividing by the surface area of the ice. Then, the stream-wise component of the ice weight was subtracted for all tests and its value was found to range from 30 to 165 g (0.66 lbf to 0.363 lbf) depending on the total ice mass on the water surface slope of 5 x 10⁻⁵. The total measured load varied from 150 to 400 g depending upon the shear stress and total ice mass.

Two techniques of isolating the ice cover were evaluated and both gave good results. The first technique was used with the plastic "ice." The instrumented and floating ICS prevented the ice from moving downstream, while another floating ice boom surrounded the ice floes upstream and was connected to the outside ICS force measuring rods. This outer boom prevented the ice from coming in contact with the shoreline. The shear stress measurements for a flow of 5950 m³/s (210,000 cfs) were reproduced with good results that scaled up to prototype values. The first test with the U.S. portion of the ICS in position 1 (see Fig. 19) had four separate measurements taken for the shear stress and produced a scaled-up value of 1.28 N/m² (0.027 lbf/ft²). The second test, repeated four days later but on position 2 (Fig. 19) gave a value of 1.29 N/m² (0.027 lbf/ft²). The shear stress for a flow of 4700 m³/s (166,000 cfs) at 578.1 ft was also measured. It gave a value of roughly 1.81 N/m² (0.038 lbf/ft²).

The second technique used a solid ice sheet covering only a portion of the model. The ice cover shear stress for a solid ice sheet could be measured without attaching a surrounding boom by physically moving the large sheet (~ 6 x 6 m) to different sections of the model and letting the floe come to rest against the ICS. The shear stress computed was 1.38 N/m² (0.029 lbf/ft²). The floe extended from the Canadian ICS to range 4 in the model.

Moving this floe to the center of the navigation track with its boundaries between ranges 22 and 17 resulted in a shear stress of 2.23 N/m² (0.047 lbf/ft²), a value very consistent with the equivalent prototype measured conditions at sites 32 and 55. The values of the shear stress are high because the ice floe being used had remained after a series of tests and the underside had roughened due to melting caused by warm water at 0.4°C entering the inlet trough.

Once the readings were completed for determining the shear stress values, the upstream ice boom surrounding the ice floes was removed and the ice was permitted to come into contact with the shoreline so that force readings could be obtained in this situation. To ensure that the ice had sufficient contact with the shoreline, the ice cover was surged by raising and lowering the downstream control gate, producing a small wave upstream that moved the ice cover about 1 m (3.28 ft). When the disturbance decayed, the ice floes would be rearranged and good contact would occur along the shoreline. The average load to the ice control structure with the fragmented ice in contact with the shoreline was approximately 80% of the ice-free load, with a range of 73 to 83% for four replicate tests.

Point velocity measurements were conducted under the ice at the same locations where open water and ice-covered velocity profiles were gathered. Velocity measurements beneath fragmented plastic and natural ice covers and a uniform consolidated (nonbroken) ice cover were conducted.

23

Lake Huron

16
17
18
19
20
21
22
23

θ

Michigan
USA

No. 4   US ICS

No. 3
No. 2
No. 1

USCG
Light House ▲

Canadian ICS

β

St. Clair
River

Sarnia
Yacht Club

R-12
R-13
R-14
R-15

R-11
R-10
R-8
R-7
R-6
R-5
R-4
R-3
R-2
R-1

Ontario
Canada
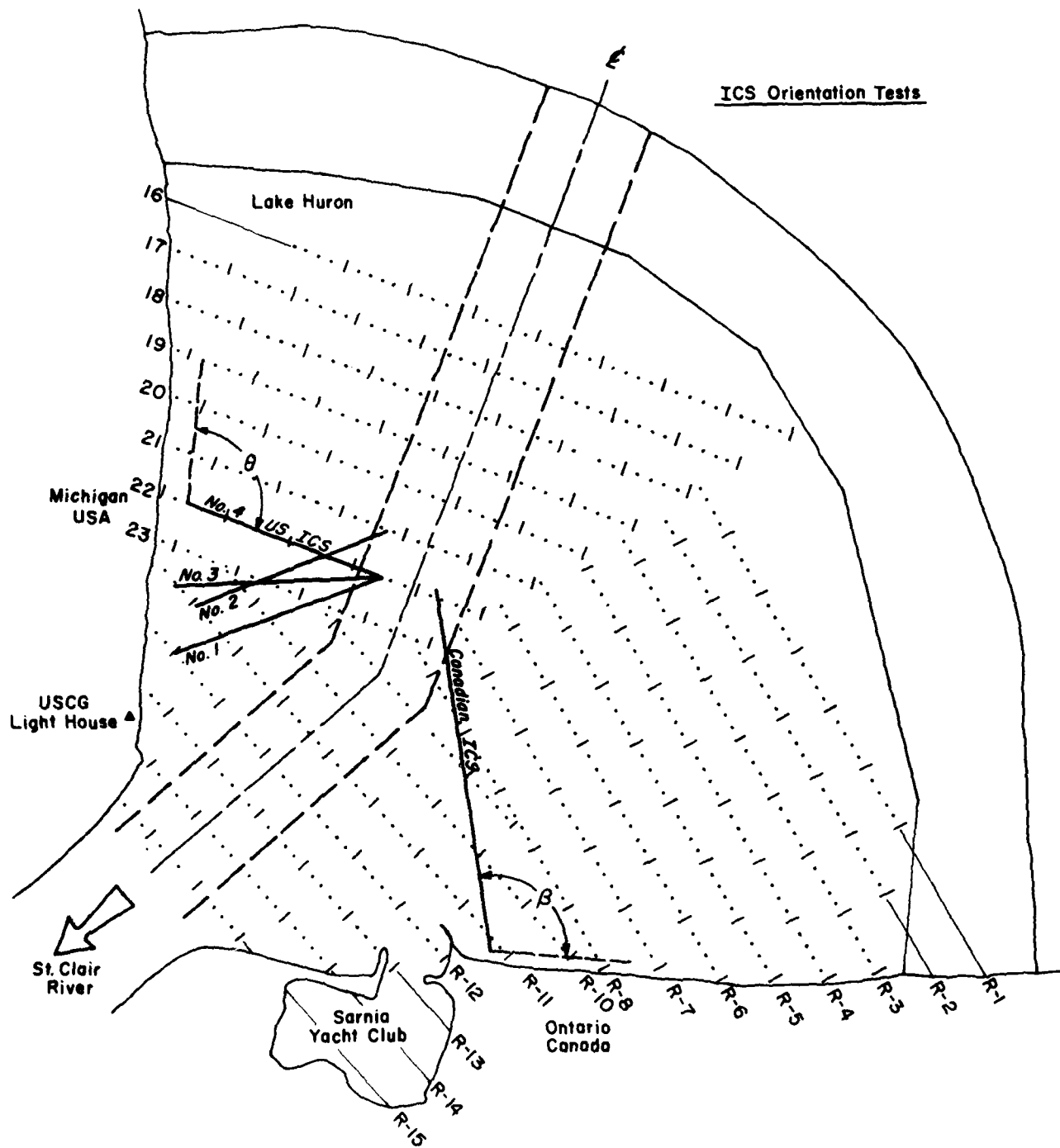
Figure 19. Ice control structure orientation positions.

24

Table 4. Mean velocity measurements beneath ice cover of fragmented square plastic floes.

	Flow rate		Flow rate	
	5950 m^3/s (210,000 ft^3/s)		4700 m^3/s (166,000 ft^3/s)	
	Velocity		Velocity	
Site*	(m/s)	(ft/s)	(m/s)	(ft/s)
30	0.56	1.8	0.53	1.7
57	0.59	1.9	0.68	2.2
32	0.65	2.1	0.59	1.9
55	0.62	2.0	0.68	2.2
34	0.53	1.7	-	-
36	-	-	0.37	1.2
51	0.34	1.1	0.31	1.0
49	0.34	1.1	0.31	1.0
63	-	-	0.40	1.3
61	0.31	1.0	0.28	0.9
26	0.59	1.9	-	-

* See Figure 11 for location of the sites.

Table 5. Mean velocity measurements beneath a consolidated ice cover (1 m, [3.3 ft] thick) and a fragmented freshwater ice cover (0.76 m, [2.5 ft] thick).

	Consolidated ice cover						Fragmented ice cover	
	5950 m^3/s	210,000 ft^3/s	5385 m^3/s	190,000 ft^3/s	4700 m^3/s	166,000 ft^3/s	4700 m^3/s	166,000 ft^3/s
	Velocities							
Site*	(m/s)	(ft/s)	(m/s)	(ft/s)	(m/s)	(ft/s)	(m/s)	(ft/s)
30	0.47	1.5	0.40	1.3	0.28	0.9	0.56	1.8
57	0.65	2.1	0.65	2.1	0.56	1.8	0.56	1.8
32	0.68	2.2	0.84	2.7	0.84	2.7	0.93	3.0
55	0.78	2.5	0.84	2.7	0.74	2.4	0.93	3.0
34	0.62	2.0	0.74	2.4	0.65	2.1	0.78	2.-
36	0.47	1.5	0.59	1.9	0.56	1.8	0.59	1.9
51	0.47	1.5	0.56	1.8	0.47	1.5	0.40	1.3
41	0.47	1.5	0.43	1.4	0.43	1.4	0.43	1.4
49	0.34	1.1	0.34	1.1	0.34	1.1	0.43	1.4
63	0.43	1.4	0.47	1.5	0.34	1.1	0.43	1.4
61	0.40	1.3	0.47	1.5	0.47	1.5	0.37	1.2

*See Figure 11 for location of the sites.

The plastic fragmented cover provided the more uniform condition of single layered ice floes over the entire model.

Table 4 is a summary of the mean velocities under a plastic fragmented ice cover. The two flow rates in the table show similar velocity conditions at the same sites, which are within the range of the velocity measurement equipment. Table 5 gives velocity data taken under a laboratory grown ice sheet for several flow rates using the same consolidated ice sheet. In general the mean velocity conditions are similar at each site. The velocity patterns (streamlines) with a solid ice cover were determined by injecting dye beneath the ice cover and observing its path. Figure 20 gives the drogue lines for a flow of 5950 m^3/s (210,000 ft^3/s). The patterns are generally similar to the open channel flow near the center of the lake (navigation channel), but because of the ice blockage along the shallow U.S. shoreline, the flow tends to be slightly diverted toward the navigation track by approximately 46 m (150 ft) between ranges 17 and 21.

25

Velocity Directions

Consolidated Real Ice Cover
210,000 cfs
Ice Thickness 3.3 ft

Lake Huron

Michigan
USA

USCG
Light House ▲

St. Clair
River

Sarnia
Yacht Club

Ontario
Canada

R-1
R-2
R-3
R-4
R-5
R-6
R-7
R-8
R-10
R-11
R-12
R-13
R-14
R-15

16
17
18
19
20
21
22
23
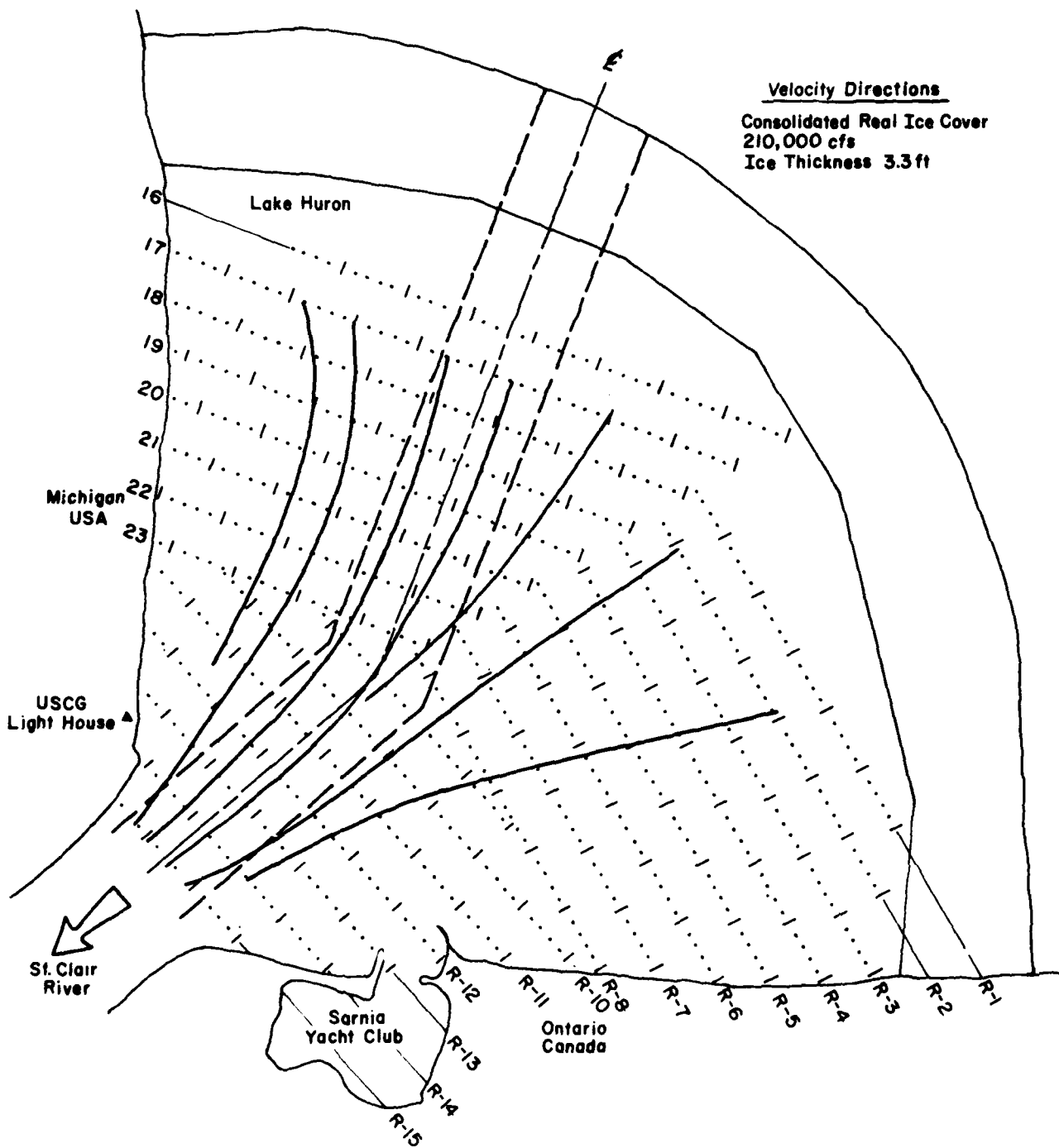
Figure 20. Drogue lines under consolidated ice cover for 5950 m³/s.
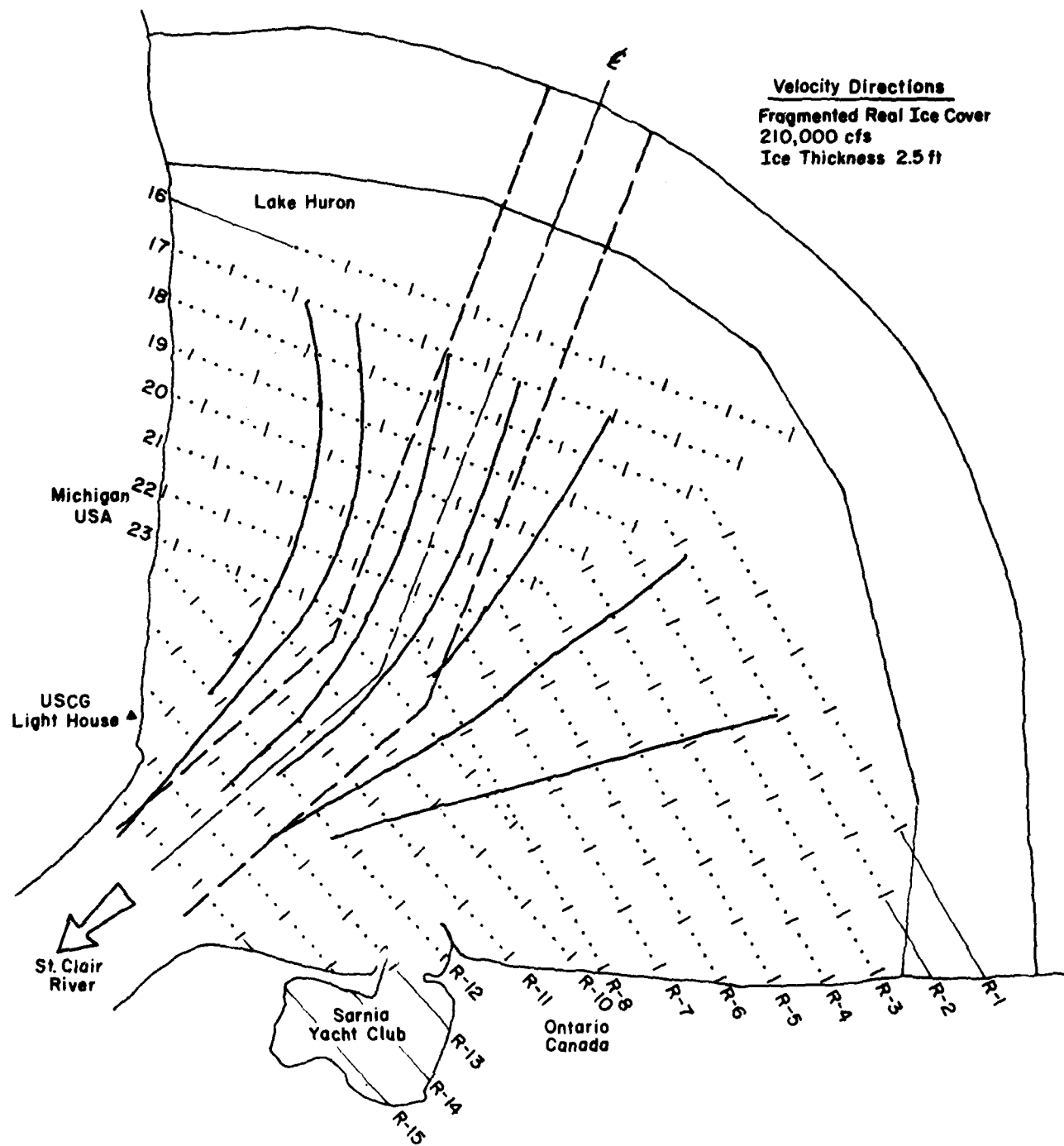
Figure 21. Drogue lines under fragmented ice cover for 5950 m³/s.

The velocity conditions changed more near the U.S. shoreline than in any other location due to the thick ice cover that moved the flow easterly into the lake. This is seen by the increase in the mean velocity at sites 30, 32 and 55 with hardly any change in mean velocities from the navigational channel to the Canadian shoreline. Figure 21 represents the stream lines beneath a fragmented ice cover. Other than the shift in the flow along the U.S. shoreline between ranges 17 and 21, there is only a small change in the flow patterns with respect to a fragmented or a consolidated ice cover.

ICE CONTROL STRUCTURE ORIENTATION

The orientation of the ice control structure was evaluated using square plastic ice floes. During these tests no discharge of the ice was allowed. The hydraulic conditions for all tests were a flow rate of $5950 \text{ m}^3/\text{s}$ (210,000 cfs) at an elevation of 176.72 m (579.80 ft IGLD) at the new Ft. Gratiot gauge. The priorities for analyzing the ICS locations were its 1) safety with respect to navigation, 2) effectiveness, and 3) minimal cost.

The navigation channel from Lake Huron makes an alignment shift of 27°, approximately 610 m (2000 ft) above the entrance to the St. Clair River. The ICS must be located upstream or downstream from the turning area to minimize or eliminate any problems associated with negotiating this turning maneuver during ice conditions. Since the downstream position is not satisfactory because of high flow velocities, the location of the ice control structure above the turning point is the only practical site.

The performance of the ICS in retaining individual floating ice floes is governed by the flow velocity, water depth and ice floe thickness one desires to contain. A summary of laboratory studies on stability of individual ice floes was provided by Ashton (1974), who recommended the following equation:

$$V_c = \frac{2(1 - t_i/H)\sqrt{(1 - \rho_i/\rho_w)\, g\, t_i}}{\sqrt{5 - 3\,(1 - t_i/H)^2}} \tag{12}$$

where V_c = critical velocity upstream of cover
t_i = ice thickness
H = flow depth
ρ_i = density of ice

If the actual flow velocity is less than V_c for the given parameters of t_i and H, then juxtaposition of individual floes will occur without rafting.

It has been observed in the field that an ice cover can form with thin 3-cm (0.1-ft) ice against flow velocities of up to 0.6 and even 0.7 m/s (2-2.3 ft/s). This implies that the cover forms a minimum thickness and progresses upstream, and the thickness is governed by a stability criterion such as the one suggested by Ashton (1974). At the beginning of the ice season, containment of thin ice floes behind an ICS will always be a problem, but once the ice floes begin to develop a thickness of 5 to 10 cm (0.15 to 0.3 ft) and attain a floe surface dimension of a few meters, ice cover thickening and uplake progression behind the boom will begin. In all model tests, the ice control structure was located in areas with flow velocities of less than 0.6 m/s (2.0 ft/s) and the cover thickness was always greater than 0.46 m (1.5 ft).

The ICS from the eastern side of the navigation channel to the Canadian shoreline is sited above a breakwater used to protect a small marina. The velocities in this area are generally low [< 0.4 m/s (1.25 ft/s)]. Also, this location should minimize problems with near-shore structures and not affect the marina operation during late fall or early spring. The position of the U.S. portion of

Table 6. Load distribution ratio on ICS at selected orientations.

Position	Test	U.S. ICS (N/m)	U.S. ICS (lbf/ft)	Can. ICS (N/m)	Can. ICS (lbf/ft)	Load ratio U.S./Can.	Orientation (°)
1	8	645	44.2	794	54.4	0.81	65
1	9	727	49.8	910	62.3	0.80	65
2	12	1197	82.0	1543	105.7	0.78	65
3	5a	1466	100.4	1637	112.1	0.90	85
3	5b	1515	103.8	1717	117.6	0.88	85
3	6a	1025	70.2	1143	78.3	0.90	85
3	6b	1048	71.8	1198	82.1	0.87	85
4	7	1231	84.3	1279	87.6	0.96	105

the ICS offered some flexibility in its orientation angle with respect to the shoreline and its uplake position.

To evaluate the U.S. section of the ice control structure, the Canadian ICS remained stationary for all tests. Since it is very difficult, if not impossible, to reproduce exactly the same ice floe positions for each test, the shear stress on the ice underside varies from test to test because of the different floe arrangements. The assumption is made that the ice conditions are generally similar over the entire model and that any change in conditions for each test is also similar over the entire model. This assumption allows us to normalize the load measured at the U.S. ICS by the Canadian ICS load. Figure 19 shows the four experimental locations for the ICS orientation test and Table 6 gives the tabulated results. The orientation angle is measured clockwise from the shoreline to the ICS as was shown in Figure 19.

Figure 22 shows quite clearly the effect of the orientation angle on the load distribution of the U.S. ICS. The smaller the included angle between the shoreline and the ICS (as shown by positions 1 and 2 in Fig. 19), the lower the load to the U.S. ICS. This interpretation implies that more of the load is being taken by the shoreline along the U.S. side. A practical limit is reached as to the minimum included angle, because the ICS must increase in length to reach the same stationary location near the navigation channel.
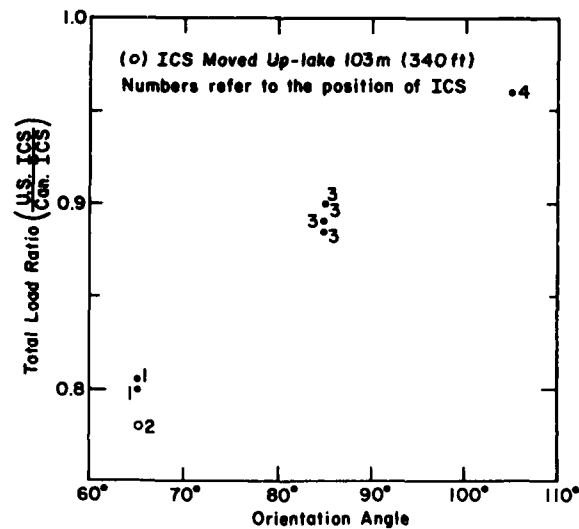
Figure 22. Results of orientation force tests—ratio of U.S./Can. loads on ICS.

29
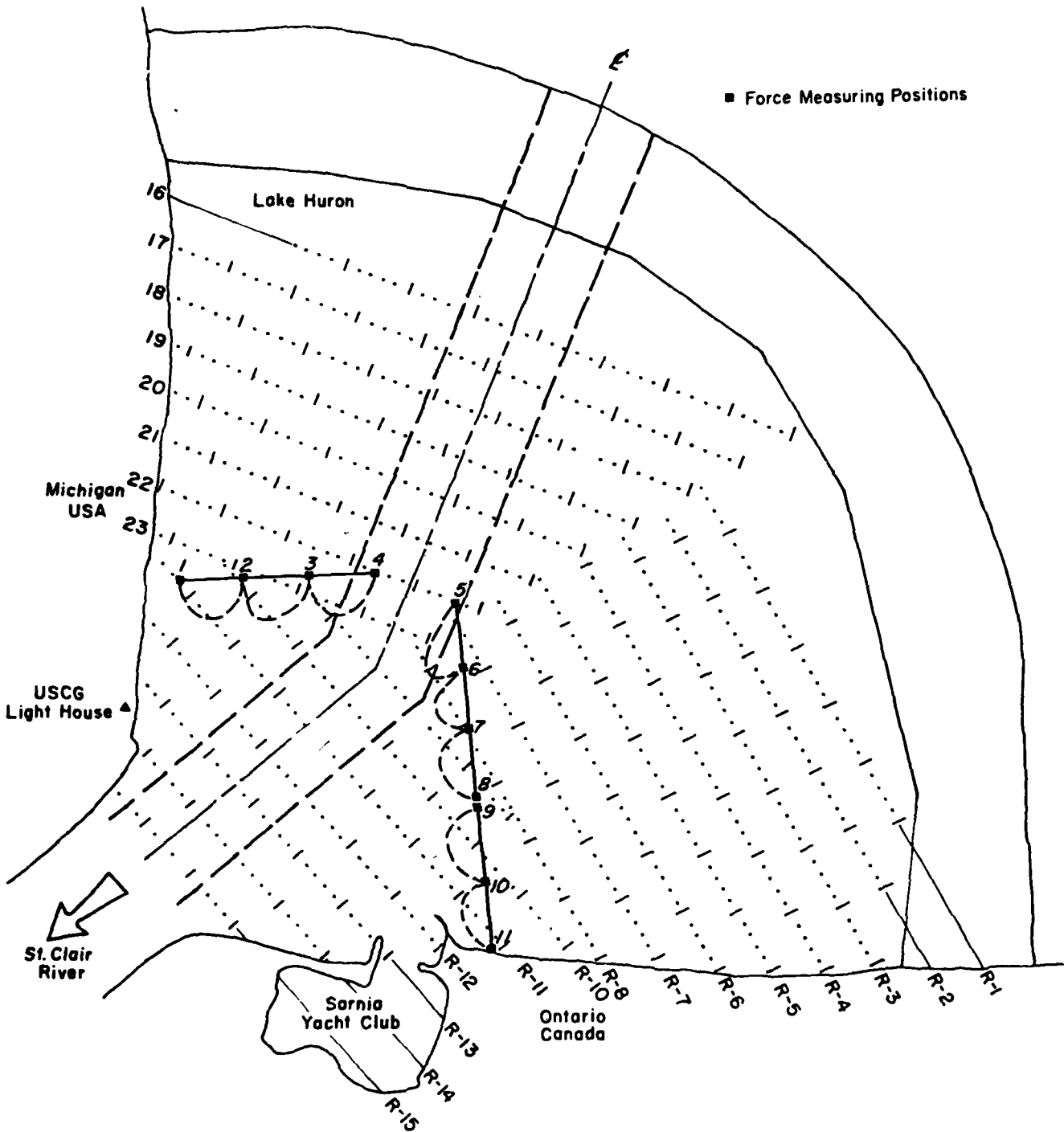
Figure 23. Force-measuring bar positions.

The conclusions reached from these tests show that the orientation of the structure should have an included angle of slightly less than 90° measured clockwise from the upstream shoreline to the ICS (i.e. it should be somewhere between position 1 and position 3 in Fig. 19).

While the same hydraulic conditions and same quantity of ice were maintained and the only difference between tests was the ice floe interaction, the resulting drag force varied by a factor of roughly 1.5 for four tests at position 3. Throughout all the orientation tests, the Canadian ICS with a constant position took loads that differed by a factor of at least 2. These few tests confirmed that many runs had to be undertaken to get a reasonable range for the force distribution in modeling as well as in the field data, since the effective shear stress appeared to be highly variable.

Once the orientation tests were completed, the location of the ICS was set according to the general alignment of position 3 in Figure 19. Table 7 represents the coordinates of the 122-m (400-ft) gap using the Michigan State Survey Coordinate System. The other gap positions may be calculated readily, as the gap kept the same bearing and its center coincided with the centerline of the shipping channel. The relative bar positions 1-11 are given in Figure 23 for all tests conducted. The intermediate locations of the force measuring rods for tests with the 122 m (400 ft) gap are also given in Table 7.

From Table 7 the positions of the measuring bars for the other tests may be calculated. The movement of these rods for all tests would be less than ± 61 m (200 ft) from their location as given in the previous table.

The difference in the total load due to the bars in slightly different locations would be negligible. Any adjustment in the load distribution would be small due to the small change in velocity between stream lines within this 61-m (200-ft) distance.

Table 7. Survey coordinates for the 122-m (400-ft) gap.

Location	Michigan state coordinates		Bar position
U.S. ICS Gap	834197	553062	4
Can. ICS Gap	834597	553082	5
U.S. Shoreline	823751	552575	1
Can. Shoreline	836175	551086	11
	833240	552715	2
	833738	552922	3
	848940	552697	6
	835244	552204	7
	835649	551799	8
	835639	551761	9
	836025	551370	10

ANALYSIS OF ICE DISCHARGE DUE TO SHIP TRANSITS

The most critical time for ice discharge through an opening in an ice control structure due to ship transits is when the ice field is in an unconsolidated state (when fragmented randomly shaped ice floes are in a random mixture). The planar dimension of these randomly shaped ice floes can vary from a few meters to hundreds of meters.

The analysis of the ice discharge due to ship transits is similar in some respects to the problem of ice arching studied by Calkins and Ashton (1975). The bleeding of ice through the gap in an ice boom after a ship transit can be a function of many independent variables:

$$A_r = f(a, b, k, V_w, \Phi, V_v, b_s, \psi, \xi) \tag{13}$$

31

where A_r = area of ice released per vessel transit

   a = average floe size dimensions from eq 11

   b = gap opening

   k = ice type and ice field conditions

   V_w = water velocity

   Φ = vessel direction

   V_v = vessel speed

   b_s = beam of ship

   ψ, ξ = orientation and geometry of the ICS.

The orientation tests performed earlier fixed the geometric parameters ψ and ξ at constant values for all the further experimental work. To study ice discharge it was decided to use a single vessel of fixed beam whose dimensions would be nearly those of the largest ships now operating in the Great Lakes. The water velocity (related to the shear stress on the ice cover) was relatively constant for the flow range considered; consequently, all tests were conducted at the maximum flow rate and maximum water levels expected at Port Huron.

The variables can be reduced to a nondimensional grouping without b_s, V_w, θ, β. The ice discharge normalized by the gap opening yields

$$A_r/b^2 = f_1 \left(a/b,\ V_s/V_w,\ k,\ \Phi,\ b/b_s\right). \tag{14}$$

Three different fragmented ice types k were evaluated: freshwater, urea-doped and polyethylene plastic. The ship direction Φ was either upbound or downbound. The ratio V_s/V_w varied over a small range, but its major influence was how the ice field was rearranged by the ship transits. The last parameter in eq 12 (b/b_s) was found to be insignificant by itself in analyzing the ice bleeding data. This reduces eq 4 and the ice discharge to a function of three nondimensional quantities:

$$A_r/b^2 = f_2 \left(a/b,\ k,\ \Phi\right). \tag{15}$$

The bleeding of ice through openings in ice booms due to ship passages has been documented for the St. Marys River by the Detroit District. The three years of record showed an average surface ice discharge of $0.35\ b^2$ per vessel passage. In an idealized flume study of ice discharge Calkins and Ashton (1975) report a value of $0.9\ b^2$ for synthetic square ice floes without regard to floe size or gap opening. Other physical model studies conducted by Acres American Inc. (1975) and Arctec Inc. (1978) report average ice discharge values of $6\ b^2$ and $2\ b^2$, respectively, for booms with a gap of 69 m (225 ft).

The effect of propeller wash on ice bleeding was not investigated because its effect would be minimal due to the limited area of the propeller in comparison to the size of the ice floes. However, another concern of some members of our staff was that the modification of ship stern and the alternating direction of ship passages could be biasing the ice bleeding data. To evaluate this possibility, the following tests were conducted with vessel transits in one direction (upstream) for 1) the ship with identical bow and stern sections (tests 76 and 77), and 2) the ship with normal bow and stern sections (test 78).

The tests were conducted using the randomly shaped synthetic ice floes with an ICS gap corresponding 91.5 m (300 ft) and similar hydraulic conditions. The results (Table 8) show that there is little difference in ice bleeding for upstream transits between a normal ship (test 78), and a ship with an identical bow for the stern (tests 76 and 77). Tests 70, 74, and 75 are alternating vessel passages and their mean ice discharge does not significantly differ from that of tests 76, 77 and 78. Test 78 reflects the ship with a normal configuration and operated in one vessel direction only. The mean discharge value lies within the range of the data taken for tests 70, 74 and 75.

Table 8. Test parameters for plastic ice floes.

Test	Ice thickness (m)	(ft)	Floe size (a) (m)	(ft)	Gap opening (b) (m)	(ft)	a/b	Remarks
15	0.54	1.8	34.5	113	189.2	600	0.188	Square floes
16	0.54	1.8	34.5	113	122	400	0.283	
17	0.54	1.8	34.5	113	91.5	300	0.377	Ice rafting noticed
18	0.54	1.8	34.5	113	198.2	650	0.174	
70	0.54	1.8	17.4	57	91.5	300	0.190	Randomly shaped floes
71	0.54	1.8	17.4	57	122	400	0.143	
72	0.54	1.8	17.4	57	152.4	500	0.114	
73	0.54	1.8	17.4	57	182.9	600	0.095	
74	0.54	1.8	17.4	57	91.5	300	0.190	
75	0.54	1.8	17.4	57	91.5	300	0.190	
76	0.54	1.8	17.4	57	91.5	300	0.190	All upbound transits
77	0.54	1.8	17.4	57	91.5	300	0.190	All upbound transits
78	0.54	1.8	17.4	57	91.5	300	0.190	Upbound using normal ship

Table 9. Test parameters for laboratory grown fragmented ice floes.

Test	Ice thickness (m)	(ft)	Floe size (a) (m)	(ft)	Gap opening (b) (m)	(ft)	a/b
24	0.94	3.1	19.7	52	122	400	0.129*
25	0.77	2.5	26.8	88	122	400	0.220†
26	1.02	3.3	27.7	91	122	400	0.225†
27	1.19	3.9	11.0	36	122	400	0.090†
28	0.72	2.4	16.2	53	91.5	300	0.176†
29	0.51	1.7	8.8	29	91.5	300	0.097†
30	1.02	3.3	12.2	40	91.5	300	0.132†
31	0.64	2.1	8.2	27	91.5	300	0.091†
32	0.64	2.1	8.5	28	91.5	300	0.093†
33	1.44	4.7	11.3	37	122	400	0.092*
34	1.11	3.6	14.9	49	122	400	0.121*
35	1.28	4.2	13.7	45	122	400	0.113†
36	0.51	1.7	15.5	51	122	400	0.127
37	0.60	2.0	12.5	41	122	400	0.101
39	0.85	2.8	9.2	30	122	400	0.075
40	0.77	2.5	13.7	45	182.9	600	0.075
41	1.28	4.2	19.8	65	182.9	600	0.108
42	1.19	3.9	33.8	111	182.9	600	0.185
60	1.19	3.9	9.0	29	91.5	300	0.098**
61	0.68	2.2	12.0	39	91.5	300	0.132**

* No ice rafting during tests.
† Ice rafted adjacent to ship track.
** Urea doped ice

All the data for the ice bleeding tests are summarized in Tables 8 through 11 for the natural and synthetic ice floes. The combined tests represent over 1000 vessel transits through the four ICS openings. In the tables, the ice discharge per vessel transit (A_r) has been normalized by the gap opening squared (b^2). For each test the mean and standard deviation of the ice discharge per vessel transit in one direction are given. Some vessel transits produced no ice discharge and the adjusted values of ice discharge with the "zero data" removed are given in Tables 10 and 11. Also computed are the exceedance levels for three frequencies of 90, 50 and 10% from a fit of the

33

Table 10. Ice discharge results for laboratory-grown fragmented ice floes.

	Ice discharge A_r/b^2			No. of tests	Skew coef.	Adjusted A_r/b^2	Sample size
Mean/std. dev.	90%	50%	10%			Mean/std. dev.	
24U 0.49/0.45	0.06	0.35	1.09	11	1.13	0.49/0.45	11*
D 0.49/0.51	0.05	0.34	1.13	11	1.43	0.49/0.51	11*
25U 0.14/0.19	0.00	0.06	0.39	19	1.27	0.19/0.20	14*
D 0.29/0.32	0.00	0.19	0.70	19	1.23	0.35/0.33	16*
26U 0.04/0.06	0.00	0.03	0.12	37	1.83	0.07/0.06	23*
D 0.21/0.27	0.00	0.13	0.51	37	2.44	0.22/0.28	35*
27U 0.32/0.37	0.02	0.22	0.74	26	1.78	0.34/0.37	25*
D 0.54/0.71	0.06	0.36	1.20	26	2.67	0.54/0.71	26*
28U 0.06/0.11	0.00	0.03	0.18	34	2.49	0.90/0.12	24†
D 0.23/0.21	0.04	0.18	0.48	36	1.47	0.23/0.21	36†
29U 0.08/0.09	0.00	0.05	0.22	15	0.18	0.11/0.08	11†
D 0.13/0.07	0.05	0.11	0.22	15	0.39	0.13/0.07	15†
30U 0.17/0.22	0.01	0.11	0.40	30	2.36	0.18/0.22	28**
D 0.37/0.39	0.07	0.29	0.78	30	2.71	0.37/0.39	30**
31U 0.06/0.06	0.00	0.06	0.14	27	0.55	0.08/0.05	27**
D 0.21/0.12	0.07	0.18	0.37	27	0.68	0.21/0.12	27**
32U 0.16/0.21	0.00	0.11	0.36	30	3.10	0.18/0.21	27**
D 0.31/0.16	0.14	0.29	0.51	30	1.49	0.31/0.16	30**
33U 0.95/0.81	0.18	0.74	1.94	16	1.26	0.95/0.81	16**
D 1.31/0.65	0.52	1.18	2.24	16	0.51	1.31/0.65	16**
34U 0.55/0.36	0.14	0.46	1.07	20	0.48	0.55/0.36	16**
D 1.38/0.95	0.52	1.22	2.42	20	2.36	1.38/0.95	20**
35U 0.23/0.34	0.00	0.12	0.59	29	2.44	0.25/0.35	27**
D 0.35/0.60	0.01	0.18	0.88	29	2.80	0.35/0.60	29**
36U 0.05/0.07	0.00	0.02	0.13	28	1.26	0.07/0.07	20**
D 0.14/0.23	0.00	0.08	0.36	28	2.23	0.15/0.23	26**
37U 0.20/0.23	0.01	0.13	0.49	22	1.28	0.21/0.23	21**
D 0.41/0.35	0.04	0.28	0.97	22	0.29	0.41/0.35	22**
39U 0.82/0.49	0.31	0.73	1.43	10	0.87	0.82/0.49	10**
D 0.80/0.57	0.18	0.65	1.61	10	0.42	0.80/0.57	10**
40U 0.32/0.23	0.05	0.25	0.68	10	0.28	0.32/0.23	10†
D 0.53/0.39	0.12	0.43	1.04	10	0.87	0.53/0.39	10†
41U 0.34/0.18	0.11	0.29	0.62	5	0.70	0.34/0.18	5†
D 1.23/0.20	-	-	-	5	-	1.23/0.20	5†
42U 0.02/0.04	0.00	0.01	0.06	20	2.21	0.03/0.04	14†
D 0.36/0.36	0.04	0.25	0.80	20	1.63	0.36/0.36	20†
60U 0.26/0.50	0.01	0.14	0.67	15	3.53	0.26/0.50	15**
D 0.35/0.38	0.02	0.22	0.84	15	1.02	0.35/0.38	15**
61U 0.17/0.38	0.00	0.08	0.44	10	3.13	0.17/0.38	10**
D 0.19/0.31	0.01	0.11	0.46	10	2.46	0.19/0.31	10**

* Static forces measured
† No data taken.
** Dynamic forces measured.

individual data by a 2 parameter gamma function . If other exceedance levels are desired, the ice discharge values can be computed using the normal Pearson Type III distribution with the data from Tables 10 and 11. See Appendix C for further explanation of the data-fitting procedure.

Table 11. Ice discharge results for plastic ice floes.

Mean/std. dev.	Ice discharge A_r/b^2			No. of tests	Skew coef.	Adjusted A_r/b^2 Mean/std. dev.	Sample size
	90%	50%	10%				
15U 0.57/0.67	0.04	0.40	1.32	20	2.36	0.60/0.68	19*
D 1.04/0.44	0.39	0.93	1.82	17	-0.59	1.04/0.44	17*
16U 0.31/0.30	0.00	0.27	0.69	20	1.30	0.42/0.28	15*
D 0.94/0.43	0.40	0.86	1.58	20	0.07	0.94/0.43	20*
17U 0:19/0.30	0.00	0.00	0.61	21	0.40	0.44/0.31	9*
D 0.80/0.45	0.24	0.72	1.46	20	0.26	0.84/0.42	19*
18U 1.74/2.29	0.08	1.02	4.36	17	1.50	1.74/2.29	17†
D 1.05/0.43	0.59	1.00	1.56	14	1.30	1.05/0.43	14†
70U 0.07/0.12	0.00	0.00	0.23	25	1.11	0.16/0.15	11†
D 0.19/0.35	0.00	0.00	0.61	25	1.39	0.39/0.42	12†
71U 0.15/0.17	0.00	0.09	0.38	25	1.00	0.19/0.18	20†
D 0.71/0.59	0.11	0.56	1.48	25	1.58	0.74/0.59	24†
72U 0.64/0.49	0.07	0.45	1.46	20	0.37	0.64/0.49	20†
D 0.97/0.94	0.22	0.78	1.92	20	2.53	0.97/0.94	20†
73U 1.42/1.30	0.10	0.90	3.40	7	0.68	1.42/1.30	7†
D 1.71/1.13	0.44	1.42	3.34	7	0.34	1.71/1.13	7†
74U 0.04/0.08	0.00	0.00	0.15	10	-0.59	0.13/0.09	3**
D 0.25/0.33	0.00	0.15	0.50	10	1.55	0.27/0.34	9**
75U 0.12/0.14	0.00	0.08	0.30	10	0.47	0.17/0.14	7**
D 0.81/0.38	0.42	0.76	1.24	10	1.54	0.81/0.38	10**
76U 0.13/0.11	0.00	0.11	0.27	20	0.97	0.15/0.10	17†
77U <0.0	-	-	-	10	-	0.08	1†
78U 0.10/0.10	-	0.075	0.24	20	0.80	0.14/0.09	14†

* Static forces measured.
† No data taken.
** Dynamic forces measured.

Natural ice

The ice discharge data were broken down into upstream and downstream vessel transits. Figures 24 and 25 show the ice discharge (50% exceedance level) as a function of a/b for downbound and upbound passages. The data appear to be scattered at first glance but this scatter can be attributed to ice floes of larger than normal dimensions. Alongside tests where the ice was very thick (> 1 m) or where ice floes were larger than 20 m, a small superscript (t or 1) is indicated, and the superscript data points appear to form an upper bound on the curves. The thicker and larger floes did not raft as easily as the thinner and smaller sized ice floes. This rafting of the ice floes enhanced the re-arching of the ice floes above the opening after each transit, thereby minimizing the ice bleeding. These rafted small ice floes acted as a very cohesive unit, merely separating and rejoining as the ship passed through the rafted ice field. The small rafted floes effectively acted as large floes instead of individual smaller ones. Figures 26a-c show a sequential view of a downstream vessel transit, while Figure 26d is a closeup of the rafted ice conditions near the ship track.

The effect of the ice field conditions on ice discharge begins to disappear when the a/b ratio is less than 0.1 of the upbound transits. The data are more greatly scattered for the downstream transits but the same trends is visible. The downstream vessel transits caused a slightly greater ice discharge for the same a/b ratio than the upstream transits because of the bow push of ice through the opening for the downbound transits. The same general trends are also apparent using the mean ice discharge or the other ice discharge exceedance levels (see Fig. 27 for upbound ice discharge at the 10% level). Re-arching of the ice field when the floe size to gap opening ratio a/b is smaller than 0.075 appears to be difficult and 0.05 is probably the lower limit for ice arching to be successful with a full ice field behind the structure.

35
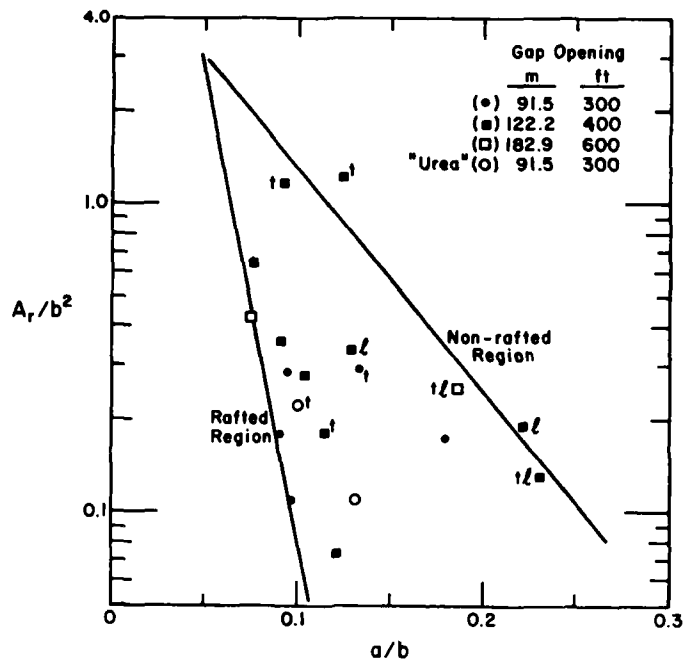
Figure 24. Downbound ice discharge—50% exceedance level—natural ice.
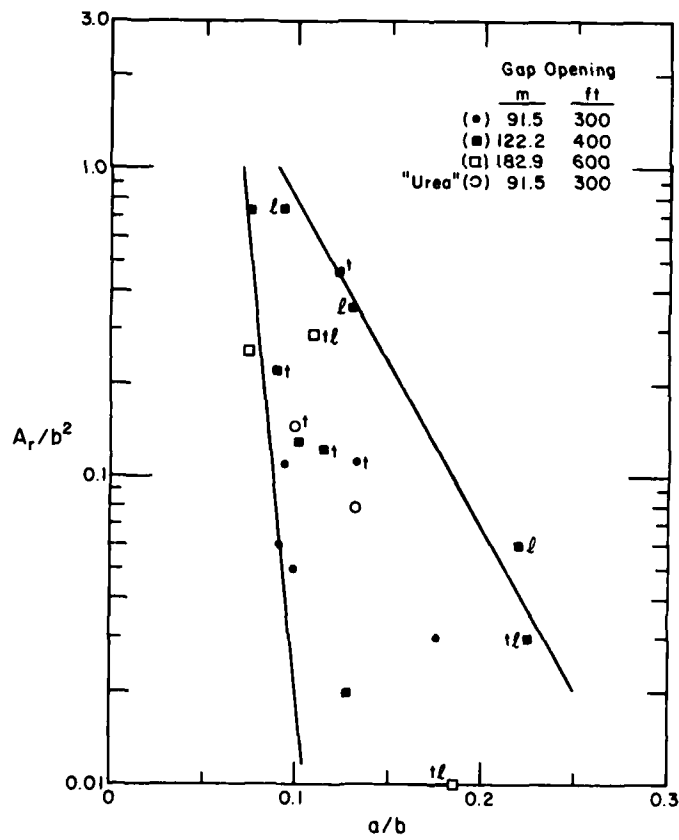
Figure 25. Upbound ice discharge—50% exceedance level—natural ice.

a.

b.
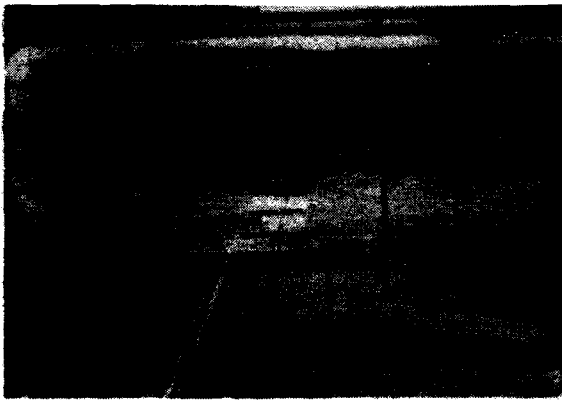
c.
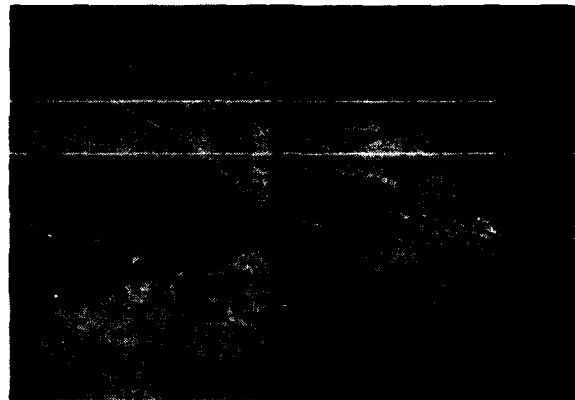
d.

Figure 26. Downbound ship transit—fragmented ice. a–c) Three sequential views of the ship transiting downstream through a fragmented ice field and the ICS. Note the relatively sharp-edged ship track. d) Close-up of the rafted ice floes adjacent to the ship track.

A general statement regarding the ice discharge is that the ice discharge occurring at 50% of the time for an unconsolidated cover will not exceed b^2, for either up or downbound vessel transits if the floe size/gap opening ratio is greater than 0.1. If the ice conditions are better documented with respect to flow size, condition of cover, etc., then a refinement in the ice discharge per vessel passage can be achieved by using Figures 24 and 25.

Figure 27. Upbound ice discharge—10% exceedance level—natural ice.

Synthetic ice

Experiments were also conducted with synthetic ice (polyethylene plastic with a specific gravity of 0.92) to determine if it could serve as a substitute for natural ice. Both randomly shaped and square uniform floes were cut from the large sheets of polyethylene. The square uniform floes of a single layer would be re-arch at a/b values less than 0.15 to 0.17; however, the randomly shaped floes re-arched at a/b values of less than 0.1. Both floes had the same prototype ice thickness at 0.54 m (1.8 ft).

The square uniform floes exhibited a much higher ice discharge for the same a/b ratio than the randomly shaped floes. Figures 28 and 29 reflect the 50% exceedance level of ice discharge for downstream and upstream transits, respectively, while Figure 30 uses the mean ice discharge of upstream transits. The mean and the 50% exceedance ice discharges reproduced identical graphs, displaced only by the skewness in the data at each a/b ratio. The ice discharge for the square uniform floes are nearly an order of magnitude greater than the randomly shaped floes.

The same trend as for the natural random floes is observed for the random synthetic ice floes: convergence of the ice discharge rate to a common value for upstream and downstream transits as the ratio a/b approaches 0.05. This is partially due to the large gap opening that allows more ice to pass through the gap opening.

Measurements on the effective depth of the ice rafting near the ship track ranged from two to four floe thicknesses and extended in scaled width up to 60–90 m (200–300 ft) on each side of the ship track centerline. This rafted zone, if greater than the opening in the ice control structure, definitely retards the ice bleeding of an unconsolidated ice field behind the structure. If the opening is greater than 120 to 180 m, the ice rafting due to ship passages is not as important a factor for reducing the ice discharge.

Figures 31a-b show the ship in the random synthetic ice field and a closeup view of the rafted ice floes adjacent to the ship track. Figures 32a-d show sequential photography of an upbound vessel transit through an ice field composed of square, uniform, synthetic ice floes.

The ice discharge data from the random synthetic ice can be overlapped with the data from the natural ice floe test. Figures 33 and 34 show the ice discharge per vessel transit at the 50% exceedance

38
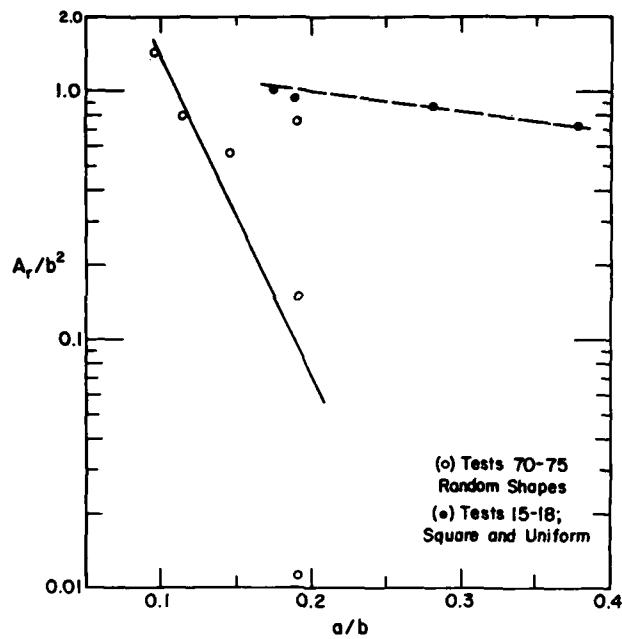
Figure 28. Downbound ice discharge—50% exceedance
level—synthetic ice.

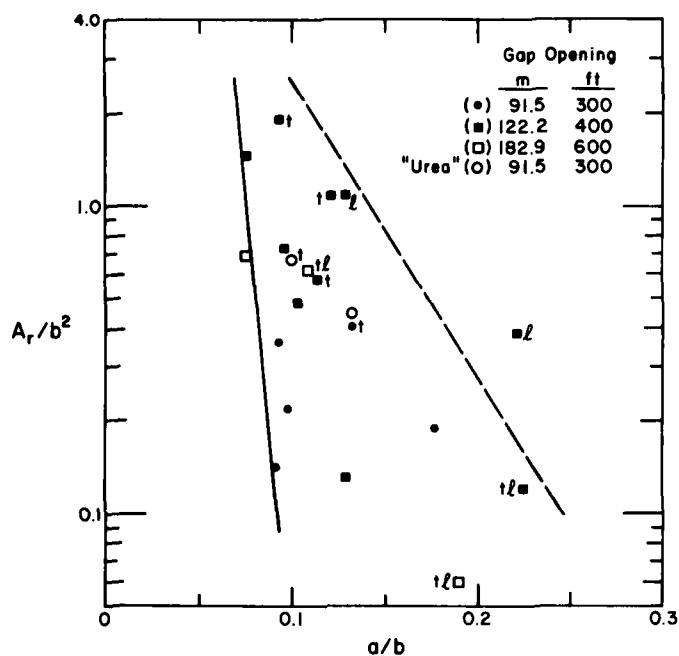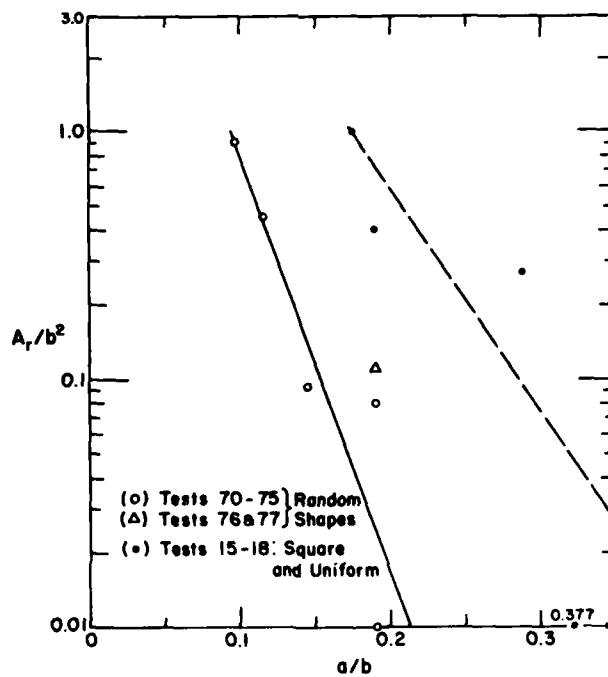Figure 29. Upbound ice discharge—50% exceedance
level—synthetic ice.

39
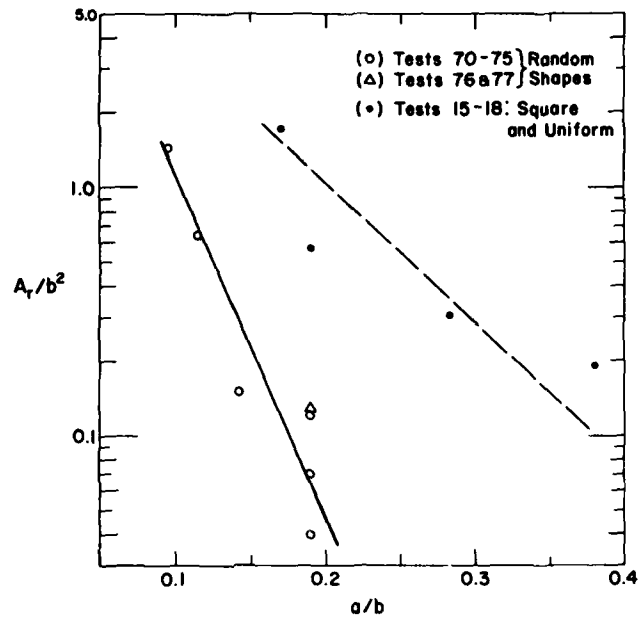
Figure 30. Upbound ice discharge—mean—synthetic ice.

a.   b.

Figure 31. Two sequential views of the ship traveling upstream through the ICS and the rafting of the plastic ice.

40
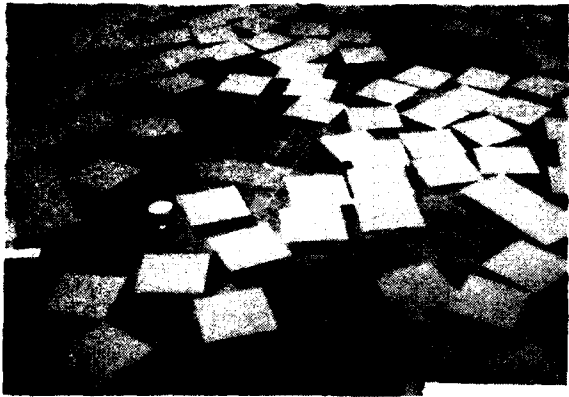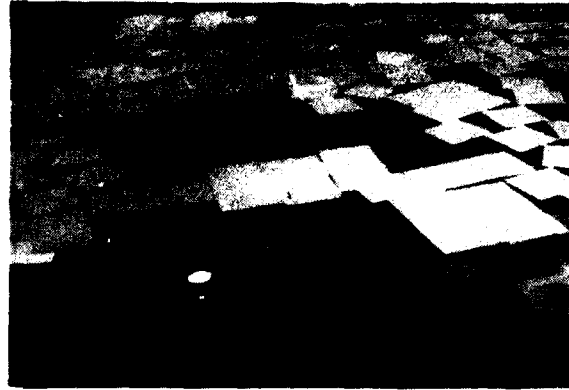
Figure 32. Sequential photos of upbound transit through square, uniform, synthetic ice floes. a–e) Six sequential views of the plastic ice discharge after the ice arch was disturbed by an upstream vessel transit through the ICS. f) Downstream view of ice discharge.

41
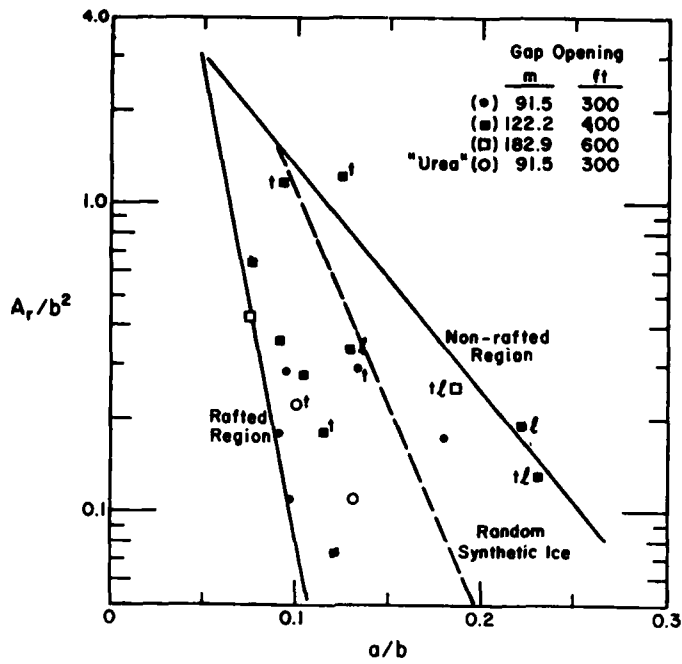
Figure 33. Downbound ice discharge, 50% exceedance level, combined natural and synthetic random floes per vessel passage.
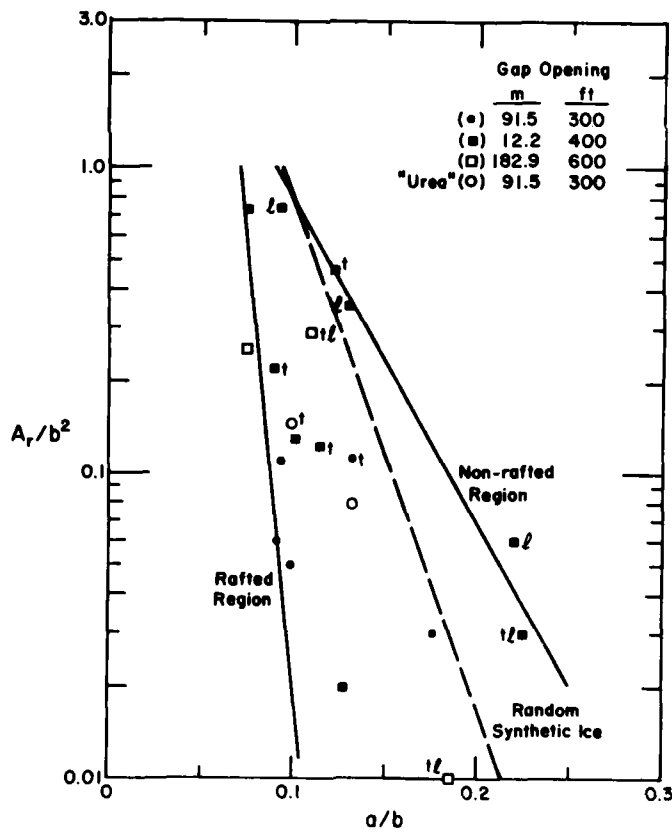
Figure 34. Upbound ice discharge, 50% exceedance level, combined natural and synthetic random floes per vessel passage.

42

level for downbound and upbound vessel transits respectively. The random synthetic ice data are represented by the solid line, which splits the envelope of natural ice data for both up and downbound transits. This similarity is very significant. In model studies of the future where ice discharge is the important parameter in the design or planning of a hydraulic structure, synthetic random-shaped ice floes may be used with assurance that they represent median conditions with respect to natural random-shaped ice floes.

FORCES ON THE ICE CONTROL STRUCTURE

The forces on the ICS were measured in two ways, depending on the type of data desired. Static force measurements were taken at the 11 bar positions prior to each ship transit through the ice field and ICS when the ice cover was stationary and no ice was flowing through the opening. The dynamic measurements of forces to the ICS began when the ship approached the ice field and continued for a period of either 33 or 50 seconds, scanning at a rate of 3 samples/second for bars 1–9.

Static measurements

The static measurements were taken to measure the changes in the overall force levels occurring after each ship passage through the ice field and ICS. Two types of ice were used, plastic and natural ice floes, and the data were evaluated in either an overall force analysis on the structure or on an individual point to point measurement basis. The overall force method resolves the forces on each of the two ICS structures to common axes. The total load is then reduced by the added force from the weight component in the flow direction and finally divided by the area of the ice cover. This yields an effective shear stress because a portion of the downstream ice load is being taken by the shoreline. A summary of the data for some of the tests is given below to illustrate the low variability within a test without physically disturbing the ice cover in the total redistributed load to the ICS for varying numbers of ship passages (Table 12).

The mean effective shear stress changes from one test to another because re-arrangement of ice floes creates a rougher ice underside either throughout the entire model or quite possibly in a localized area around the ICS and ship track. The Student's t-test done on any two pairs of data may or may not show that the sample means are from the same population. For example, runs 3 to 8, 9 to 12 and 13 to 18 in test 6 only differ in that the ice floes were repositioned in the model between

Table 12. Redistributed total force on ICS (unscaled model data)

Test numbers	Effective shear stress ± std. dev. (N/m^2)	Vessel passages	Ice type
16-3—16-7	0.0116 ± 0.0008	2	Plastic
16-3—16-8	0.0110 ± 0.0015	6	Plastic
16-9—16-12	0.0268 ± 0.0016	4	Plastic
16-13—16-18	0.0086 ± 0.0019	5	Plastic
16-19—16-25	0.0121 ± 0.0006	6	Plastic
17-2—17-7	0.0113 ± 0.0001	23	Plastic
17-8—17-11	0.0139 ± 0.0022	17	Plastic
24-5—24-8	0.0126 ± 0.0020	4	Natural
24-10—24-15	0.0133 ± 0.0019	6	Natural
25-3—25-14	0.0074 ± 0.0016	12	Natural
25-15—25-18	0.0069 ± 0.0014	5	Natural
26-4—25-14	0.0120 ± 0.0022	13	Natural
27-7—27-24	0.0265 ± 0.0021	19	Natural

tests 8 and 9, and 12 and 13. No other change occurred, yet the mean effective shear stress values differed by a factor of 2 to 3. The standard deviations were always less than 20% of the mean values for both natural ice and plastic ice, with consistent values as seen in the tables. If the shear stress values were scaled to prototype conditions, the range for the means would be 0.587 to 2.28 N/m^2, with a mean of 1.14 N/m^2, only very slightly lower than the mean value measured in the field. In other words, the measured shear stress values fall within the range of the calculated field measurements.

The distribution of load to the ICS can be broken down in terms of the forces taken at each bar. The following tables will give the average normal load at the measuring points in terms of percentage of the total normal load. The total normal load is designated as the sum of the loads normal to the orientation to each of the two ICS's. This normal load component closely corresponds to the direction of flow in the model, as the ICS was purposely situated to be nearly normal to the flow lines. In fact the loads could also be approximated in a radial configuration due to the large arc that could be constructed from the converging flow lines.

Table 13 represents the average percentage of normal force taken at each measuring position for test series 16, 17, 20, 22, 24, 25, 26, and 27. Positions 1 and 11 are nearly on shore and carried a very small percentage of the load because the ice grounded along the shoreline and transmitted the load to the shore and bed. Position bars 2 and 10 are located farther into the lake and carried loads equal to 10% and 6% of the total, respectively.

The two rods that were adjacent to the ship track (4 and 5) measured roughly 10% each of the total load. The largest loads were taken by rods 3 and 6 (21 and 16%) which were one position away from the ends of the U.S. and Canadian ICS, respectively. This was not unexpected as rods 3 and 6 have more effective ice boom lengths than rods 4 and 5. The remaining two rods along the Canadian ICS measured 13% each of the total load. Overall 42% of the mean load was taken by the U.S. ICS and 58% by the Canadian ICS, but variations would occur within each test. The maximum percentage measured for one side of the ICS within one of the runs was 58% taken by the U.S. side, and 70% for 1 run by the Canadian ICS. No distinction was made between upbound and downbound vessel transits for these data.

These percentages can be further analyzed at a local level by considering the maximum percentage taken by any one measuring position during all of the 112 vessel transits for these 8 tests. Table 14 gives the maximum percentage taken by any rod during all of these runs. Position 3 during one of the 10 runs in test 22 took 55% of the total measured load for that run. The next highest percentage was 34% taken by position 8-9. The remaining positions, excluding the two end rods, had maximum percentage loads ranging from 22% to 32%. These loads represent redistributed static loads on the structure after a vessel has transited through the ICS.

Table 13. Average percentage of total normal force taken at each position.

Test	1	2	3	4	5	6	7	8-9	10	11	No. of runs
16	3	14	16	9	8	8	12	12	17	0	10
17	5	10	18	17	4	13	8	18	7	0	23
20	0	5	22	9	9	15	13	22	6	0	8
22	2	9	23	14	5	10	18	13	7	0	10
24	0	7	19	14	8	20	10	20	3	0	11
25	2	13	30	13	6	18	12	3	2	0	16
26	1	10	25	19	6	16	21	2	0	0	11
27	0	10	12	8	14	24	12	11	8	0	23
Ave.	2	10	21	11	8	16	13	13	6	0	112

44

Table 14. Maximum percentage of normal load taken after
any run within each test. (The maximum value in each
column is italicized.)

Test	1	2	3	4	5	6	7	8-9	10	11
16	8	16	22	13	13	12	19	22	*22*	0
17	*11*	16	21	19	9	19	10	21	12	0
20	0	7	35	15	13	20	15	24	9	0
22	5	15	*55*	23	10	18	31	26	13	0
24	0	10	23	21	12	30	18	*34*	4	0
25	3	*26*	49	*27*	10	25	21	7	10	0
26	2	15	38	24	17	28	*32*	5	0	0
27	1	15	17	16	*25*	*32*	15	14	10	0

Dynamic force measurements

As mentioned earlier, continuous data were taken on the forces generated by a ship moving
through the ice field and the ICS opening. Tests were conducted with fragmented floes of plastic,
freshwater ice and doped urea ice. Only the urea-doped ice tests will be described, as the flexual
strength was scaled according to values of typical freshwater ice, 6 to 7×10^6 Pa. Comparison
between the ice types has not been completed.

Table 15 is a summary of the dynamic data taken during test 61 for 20 vessel transits, 10 up-
bound and 10 downbound. Each run consists of measuring the two-directional force 150 times
for each position (1-9) during a 50-s time frame. The vessel could traverse up or down through
the ice field and ICS in about 20 s depending on the ship speed setting. The values in Table 14
represent the ratio of maximum load recorded to the mean load for the 10 runs in both directions;
i.e. the sample population is 1500 readings per bar per direction. The x direction represents the
normal load registered to the ICS while the y direction reflects the traverse loading at each point.
Due to the relatively symmetrical pattern offered by the ICS and its relation to the flowlines, the
y-direction loads were considerably lower than the x-direction loads.

The ratios are generally consistent except for the y direction at position 3 and both x and y
directions at position 9. This basic data show that the primary reason for the large ratios at posi-
tions 3 and 9 are the relatively low mean values. Measured values for some of the runs constituted
loads of less than 2 g (or less than 2700 lbf prototype).

Table 15. Ratio of peak load to mean load for urea-
doped ice at each measuring position. Data were
taken during test 61 for 10 upbound and 10 down-
bound vessel transits.

Bar	10 upbound		10 downbound	
	X Max/mean ratio	Y Max/mean ratio	X Max/mean ratio	Y Max/mean ratio
1	1.4	2.6	1.8	4.9
2	4.2	3.8	3.8	4.2
3	22	>10	1.6	>10
4	1.9	3.6	3.4	4.7
5	2.3	2.6	1.9	1.8
6	1.9	2.2	1.8	2.2
7	1.7	1.9	1.5	1.8
8	2.4	2.9	2.1	2.0
9	>10	9.3	>10	>10

The two major conclusions drawn from Table 14 are 1) there is little difference in the ratio of the peak to mean loads for upbound or downbound ship passages at each position and 2) the ratios also appear to be relatively consistent from position to position.

These data suggest that the vessel-ice-floating structure interaction is independent of vessel direction. The rearrangement of the ice floes caused by the vessel is the dominant dynamic loading feature with a fragmented ice cover. This same conclusion (loads applied to the ice boom are independent of vessel direction) was observed for the St. Marys River ICS by Perham (1978). The dynamic load to the ICS in terms of its static load offered by the ice cover should average on the order to 3 to 5 times the static load conditions, but extreme values of greater than 10 were noted.

The information given in Tables 12–14 may be applied in determining the load on the ICS due to the ice cover water drag and ship interaction with the fragmented ice cover. Once the loading to the structure on a force per linear dimension basis (i.e. lbf/ft or N/m) has been determined, the load distribution can be computed from Tables 12 and 13. When the load distribution has been calculated, the dynamic load factors from Table 14 can be applied to each position to account for ship-ice-structure interaction at each loading position. A factor of 5 would appear appropriate for all positions.

The effect of a strong wind on the force distribution of the ICS with a ship running through a solid ice cover was not considered in the physical model, although inferences on these effects can be provided. The ship-ice floe interaction is a very localized phenomenon and any additional wind stress would be acting over a very small area of floes disturbed by the ship passage. It is our belief that the effect of wind on the interaction between the ship and the ice cover with respect to the dynamic loading would be minimal at the ICS due to the very local conditions.

POTENTIAL ADDITIONAL SHEAR STRESSES

Since the size of area to be modeled was restricted by the building dimensions, the influence of the other portions of the lake on the shear stress was evaluated mathematically. A logarithmic velocity profile distribution was used with the maximum velocity taken at $0.75D_i$, where D_i is the depth of flow. The roughness height k_i was taken as 1.5 cm (0.05 ft). The velocity profile data taken at Port Huron suggested these values (which are conservative).

An idealized situation of flow in the lake was mathematically represented. The discharge was assumed constant at 5667 m³/s (200,000 ft³/s), and the flow depth increased linearly from 6 m (20 ft) at 1.6 km (1 mile) into the lake to a depth of 15 m (50 ft) at a distance of 29 km (18 mile) into the lake. The effective width of the proposed ICS from shoreline to shoreline was estimated at 1220 m (4000 ft). The shear stress was calculated by using eq 5 over an incremental lake length of $\Delta L = 1140$ m with an effective width of 120 m (see Fig. 35). The downstream force F_i, the product of the shear stress on the ice cover τ_i and the ice cover area A_i, is summed for each successive ice cover length (j increment) extending into the lake:

$$F_i = \sum_{j=1}^{n} \tau_i^j \, A_i^j . \tag{14}$$

The calculation was halted when

$$\frac{F_i^j - F_i^{j-1}}{F_i^j} < 0.01 .$$

There are no field data available at this time to confirm the assumptions made on the velocity or shear stresses this far into the lake. The purpose for this calculation was to estimate the relative

46
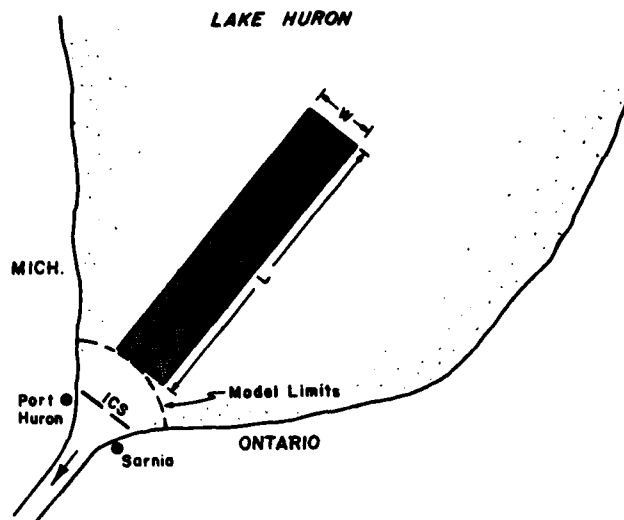
Figure 35. Schematic view of additional water drag components.
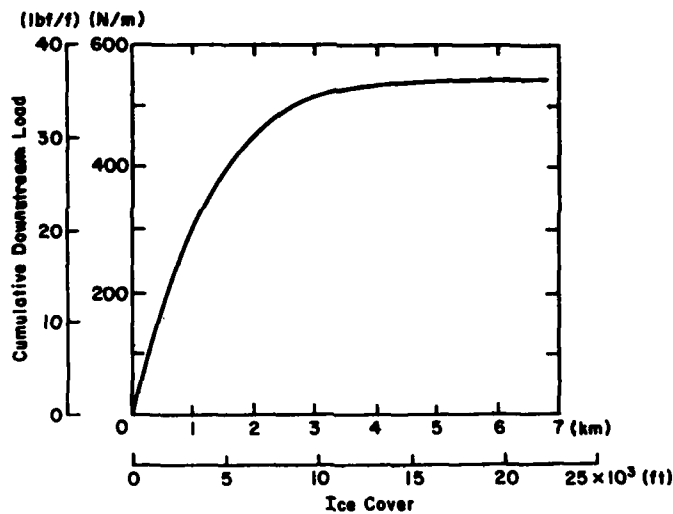
Figure 36. Estimated load to ICS with surface area not included in the model limits.

magnitude of the possible additional load due to an ice cover by the water shear stresses outside the limits of the model area.

Figure 36 shows the results of using eq 14 with the assumptions given earlier. The additional load decreases quite rapidly with distance away from the ICS; the 1% level is calculated to be approximately 5.69 km (18.675 ft) outside the limit of the model. This additional load is relatively small, only 48.8 N/m (36 lbf/ft) for an ICS with a length of 1220 m (4,000 ft). This calculation assumes that no load is taken by an arch or through shear along the ice/ice interface boundary. This additional load is an upper bound on the additional load due to water stresses not considered in the model due to space limitations.

ANTICIPATED ICE CONDITIONS WITH ICS

The ICS will undoubtedly initiate an ice cover as soon as the first ice appears at Port Huron. The ICS will change the local ice conditions along the U.S. and Canadian shorelines so that 1) the ice will form earlier and the thickness of shore ice pileup may increase, 2) the distribution and thickness of shore ice pileup will be altered, and 3) the extension of the present shear walls and shore-fast ice near the inlet to the river should move into the lake and then taper back to their present location within 1 to 2 km upstream of the ICS along each shoreline (see Fig. 8). The un-rafted zone of ice beyond the shorefast ice would be free to move uplake if a sufficient shear stress were available. The shorefast ice would not be moved uplake due to its anchored resistance along the shoreline and bed. The returning ice from uplake would then strike and arch between the shorefast ice. The shoreline, being the most rigid component of the shorefast ice, ICS and shore-line system, would absorb the majority of the load.

To minimize forces on the ICS, the shorefast ice should remain in place to serve as the buffer strip between large ice floes arriving from uplake and the ICS. The present observation of ice along the shoreline confirms the hypothesis that the shorefast ice remains until the very end of the season. With an ICS restricting its movement downstream, the ice will remain in place until it melts or is destroyed by open water wave action.

The ship passages through the ICS will affect the ice conditions upstream. The ship track will become clogged with brash ice at times. Open leads will also develop behind the ICS, both within the ship track and in other areas. These open leads, possibly extending up to 1 km in length, will be confined by the shear walls of the shorefast ice. The open leads will form by repeated ship traffic, causing small amounts of ice to pass through the opening, or possibly from thermal melting of the ice underside.

Downstream ice conditions in the St. Clair River will be altered by prohibiting ice discharge from Lake Huron. Assuming an average thickness of 15 cm (6 in.) over the ice season and the average seasonal ice discharge of 900 km^2, about 1.35×10^8 m^3 of ice would be held back by the ICS.

CONCLUSIONS

The results of this modeling effort have led to the following general and specific conclusions re-garding modeling of an ICS in a subzero environment.

1. Special construction considerations have to be used for the bed of the model. Use of fiber-glass resin only or swimming pool paint over the conventional sand-base mortar skin will work well.

2. In the open water calibration, downstream adjustments at the gate did not affect upstream flow conditions near the ICS or navigation channel and only at the inlet were adjustments possible. Flow acceleration toward the opening was dominant, and the flowlines were found to be very sim-ilar for all flows evaluated.

3. The ice cover calibration was achieved by obtaining a properly scaled shear stress which was close to the mean of data collected in the field. The many tests showed a wide variation in the shear stress values, which were calculated from direct measurements of force and divided by the ice surface area. Both plastic and natural ice offered the same effective shear stress, both having the same absolute range of values, from roughly 0.007 N/m^2 to 0.027 N/m^2. Repetitive testing was therefore found to be an absolute necessity.

4. For the random-shaped natural floes, the ice conditions upstream of the structure, the floe size/gap opening ratio (a/b), and the vessel direction were the predominant independent variables affecting the ice discharge per vessel transit (A_r/b^2).

a. The surface conditions of the ice floes upstream of the ICS (i.e. whether the floes were rafted or not) was very dominant, as a non-rafted ice field exhibited two- to five-fold greater ice discharge per vessel transit than a rafted ice field for similar hydraulic and ICS conditions.

b. The ratio of floe size to gap opening a/b was very significant in determining the ice discharge. A change in this ratio from 0.1 to 0.2 showed a 10-fold decrease in the ice discharge per vessel transit, regardless of direction. When the ratio a/b was greater than 0.25, the discharge was very minimal (<0.10 for the 50% exceedance level). The minimum a/b ratio for re-establishing a stable arch with rafted floes was approximately 0.075. The non-rafted floes approached a minimum ratio value of 0.10.

c. For the non-rafted ice fields, downstream vessel transits had generally higher ice discharges than upstream transits, primarily due to the bow push of ice through the opening.

d. The thicker and larger ice floes used in these tests did not raft as easily as the thinner and smaller sized floes. These tests indicated floes with scaled sizes greater than 1 m thick and 20 m to a side did not raft as quickly, if at all. When the width of the rafted ice zone adjacent to each side of the ship track was less than the width of the gap opening, the effects of the rafted floes in reducing the amount of ice discharged were not always significant. The scaled width of rafted ice was generally 60 to 90 m (200 to 300 ft) from each side of the ship track centerline, for a 120- to 180-m total effective width.

5. The two synthetic ice floe types (random and square shaped) displayed large differences in ice discharge for similar flow and gap opening conditions with respect to the vessel direction and the flow size to gap opening ratio.

a. The downstream vessel transits exhibited higher ice discharge per vessel passages than upstream passages for both square and randomly shaped floes. The downstream transits through the randomly shaped floes showed a 50% increase in ice discharge over the upstream passages. The randomly shaped synthetic floes exhibited ice discharge values similar to those of the randomly shaped natural ice floes. Both upstream and downstream curves for the synthetic random floes lie within the bed of data for the natural randomly shaped ice floes.

b. The square uniform size ice floes exhibited a significantly higher ice discharge by a factor of 10 than the randomly shaped floes. The downstream ice discharge for square floes was entirely controlled by bow push when $a/b > 0.20$.

c. Square uniform synthetic floes are significantly different in their ice discharge characteristics, not rafting as easily and not being able to re-arch at $a/b < 0.15$. Random synthetic floes would re-arch at $a/b \simeq 0.1$, a value slightly higher than that for natural floes.

6. The forces to the ice control structure from the ice sheet varied considerably from test to test. Both plastic ice floes and natural ice floes exhibited the same range of effective shear stress values.

a. The average percentage of the total normal load taken by each of the measuring bars, exclusive of the two end points, was generally 10 to 15%, except for one bar (3) which took roughly 20%. This bar was situated in the model where the water velocity was very high compared to the other bars.

b. The maximum normal load, as a percentage of the total load taken by any one bar during the 112 tests, was 55% by bar 3. The other remaining eight bars (2, 4, 5, 6, 7, 8, 9, 10) took between 22 and 34% of the total load during any one test run.

c. The dynamic loads registered by the 11 bars in the x-direction (i.e. parallel to the flowlines) was three to five times the average load for a particular run. The level of the dynamic loads measured was independent of the vessel direction. Downstream vessel transits did not create higher dynamic loads.

7. Future model studies that need to know only the ice discharge rates through surface openings may use synthetic ice cut into randomly shaped sizes. The polyethylene plastic of 0.92 specific density is a good substitute for natural ice for ice discharge studies.

49

8. The model results for average ice discharge per vessel transit are consistent with the field data obtained from the St. Marys River. The only field data on ice discharge averaged 0.35 b^2 per vessel passage in the St. Marys River while the physical model ranged from 0.1 to 1.0 b^2 depending on the ratio a/b, ice type, ice conditions upstream of the boom and vessel direction. This close agreement with the field data gives confidence that the modeling effort was successful for both randomly shaped natural and synthetic ice floes.

9. The orientation of any structure placed at Port Huron should be similar to the testing orientation, normal to the flowlines. The gap opening of 122 m (400 ft) works well and it offers a larger margin of safety (from ship damage) than a 61-m- (20-ft-) wide opening.

LITERATURE CITED

Acres American Inc. (1975) Model study of the Little Rapids Cut area of the St. Marys River. U.S. Army Engineer District, Detroit.

Arctec, Inc. (1978) St. Lawrence River ice boom modification study. Draft Report 281-2.

Ashton, G.D. (1978) River ice. *Annual Review of Fluid Mechanics*, vol. 10, p. 369–92.

Calkins, D.J. and G.D. Ashton (1975) Arching of fragmented ice covers. *Canadian Journal of Civil Engineering*, vol. 2, no. 4.

Pariset, E. and R. Hauser (1961) Formation and evolution of ice covers on rivers. *Transactions of the Engineering Institute of Canada*, vol. 5, no. 1, p. 41–49.

Perham, R.E. (1978) Performance of the St. Marys River ice booms, 1976–77. CRREL Report 78-24. ADA061431.

Thom, H.C.S. (1957) A note on the gamma distribution. *Monthly Weather Review*, vol. 86, p. 117–122.

U.S. Department of Commerce (1970) Handbook of mathematical functions. National Bureau of Standards, Applied Mathematics Series 55.

APPENDIX A. APPLICATION OF MODEL RESULTS

This section is written for the user of the results derived from the two model studies and the other non-modeling efforts. The majority of the data was purposely non-dimensionalized for easier interpretation at this stage in the report. The detailed design of the ICS will be done by another agency, but the basic design criteria, loads and ice discharge through the ICS are contained in this section.

The opening in the ICS will allow for vessels and ice to pass through the gap. If the ice field conditions, vessel direction and gap opening are known, the amount of ice passing during vessel transits can be calculated. The ice cover conditions at Port Huron can be highly variable, from a solid cover one day to fragmented broken floes the next. The worst condition for ice bleeding under natural and ship-disturbed conditions would be the prevalence of small fragmented ice floes whose size to gap opening ratio is less than 0.1. These particular conditions are difficult to control, but fortunately they occur only a small percentage of the time. Currently, a solid ice cover of Port Huron does not always release ice downriver when disturbed by ship transits. The photographic documentation brings this point to light.

If the ice conditions at Port Huron can be forecast, observed or measured similarly to the documentation of ice conditions in the model, detailed use of the model ice discharge figures is justified. If the ice conditions are too variable, then a conservative approach can be used to estimate ice discharge through the opening.

Example 1: A decision was reached to design for a gap opening of 122 m (400 ft). Determine the amount of ice bleeding for 100 round-trip vessel passages.

Procedure
1. Determine the ice field conditions for the winter season in terms of floe size.
2. Determine the number of ship passages for each floe size category.
3. Determine the 50% level of ice discharge per vessel transit and multiply by the number of upbound and downbound transits for each floe size to gap opening ratio.

Solution 1
1. Assume three ice field conditions
   a. 20 days, $a = 15$ m—non-rafted .... January
   b. 40 days, $a > 30$ m—rafted .... January–February
   c. 30 days, $a = 20$ m—non-rafted .... March
2. One hundred round-trip vessel transits
   a. 40 .... January
   b. 20 .... January–February
   c. 40 .... March
3. Use the upper and lower boundaries in Figures 24 and 25 for non-rafted and rafted ice fields, respectively.
   a. $a/b = 0.13$—non-rafted
      $A_r/b^2 \approx 10$ and $A_r/b^2 \approx 0.5$ (up and down)
      $A \approx 40 \times (122)^2 [1.0 + 0.5] = 0.89$ km^2
   b. $a/b = 0.25$
      A_r/b^2 0.02 and 0.05   (up and down)
      A_r $20 \times (122)^2 [0.02 + 0.05] = 0.02$ km^2
   c. $a/b = 0.16$
      A_r/b^2 0.5 and 0.2   (up and down)
      A_r $40 \times (122)^2 [0.5 + 0.2] = 0.42$ km^2
                            Total   1.33 km^2

Solution 2

One could use a maximum value of approximately 1.5 for the ice discharge regardless of vessel direction and calculate an upper bound condition.

Ice released = $100 \times (122)^2 [1.5 + 1.5] = 4.46$ km^2 (1.7 mile^2)

Example 2: What would be the ice discharge through the gap opening under natural conditions without ship transits and before the ice arched?

A solid ice cover could not be considered, only the fragmented cover. The ice floe size to gap opening would have to be small, i.e. < 0.1, and a very low ice concentration of floes at the gap. This condition would be most prevalent during freezeup or after an ice breakup due to wind action. A conservative time duration over the entire winter season might be 20 days, and 10% of the time the ice concentration might be as great as 0.5 before arching. Using a transport water velocity of 0.6 m/s (1.85 ft/s) through the gap

$$A_n = 20 \times (10\%) \,[0.5]\, 122 \text{ m} \times \frac{0.6 \text{ m}}{s} \times \frac{86400 \text{ s}}{\text{day}}$$

$$A_n = 6.3 \text{ km}^2 \ (2.5 \text{ mile}^2).$$

Example 3: What effects would wind have on the ice bleeding under natural conditions and during ship transits?

1. Ice bleeding under natural conditions will continue until the ice discharge or ice concentration at the gap opening for a given *a/b* ratio exceeds a critical value as determined by Calkins and Ashton (1975). The velocity and direction of the moving ice floe is dependent on the shear stress offered by the water and/or wind.

The ice concentration at the gap is independent of the ice floe velocity or direction. Consequently wind will have little direct effect. If waves in an open-water environment are set up by the wind, the ice will tend to move along the opposite shore or ice edge. This would impose a nonuniform ice concentration at the gap opening, and the re-arching conditions would be unfavorable. Only when the ice reacts with both ice edges along the opening will the arch form.

2. Evaluating the effect of wind on the ice discharge during ship transits follows the same line of reasoning given above. The disturbed ice field is very small and re-arching of the ice floes is dependent upon the floe size/gap opening ratio, floe conditions and to some extent the vessel direction.

Example 4: What are the design loads to the ICS from the water-induced forces and how are they distributed?

1. The ICS is sited normal to the direction of the flow and this is the optimum condition. The shear stress developed on the ice sheet resulted in loads of 650 N/m (45 lbf/ft) to 1825 N/m (125 lbf/ft) of ice control structure length. The additional load to the structure for the area not included in the model could reach another 450 N/m (30 lbf/ft). This gives a total static load of roughly 2190 N/m (150 lbf/ft) of ice control structure length.

2. The two ice control structures (U.S. and Canadian) are 465 and 755 m long respectively for a total length of 1220 m.

    a. L_T = total load = 1220 m × 2190 N/m = 2672 kN

       U.S. = 43% (L_T) = 1149 kN

       Canadian = 57% (L_T) = 1523 kN.

    b. The ratio of each ICS length to the total length is another check on the ICS load distribution, if a relatively uniform load distribution from the ice fields is assumed.

       U.S. = $\dfrac{465}{1220} \times 2671.8 = 1018$ kN

       Canadian = $\dfrac{755}{1220} \times 2671.8 = 1654$ kN .

The load distribution is consistent for both methods.

Example 5: The location of the ICS will be moved to a different position than that tested in the model. What corrections to the data need to be made?

1. The ICS is in a minimum downstream location along the U.S. shoreline. It would be possible to shift the Canadian ICS downstream until a velocity of 0.6 to 0.7 m/s (2.0–2.3 ft/s) is reached.

2. The change in the loading to the ICS can be calculated by multiplying the average shear stress over the change in surface area to account for inclusion or omission of extra load. The increase in load assuming a 200-m position movement downstream is roughly 100 N/m, i.e. less than 5% of the total used in example 4.

3. The ice bleeding would be barely affected unless the submergence velocity in the gap region was exceeded for a particular floe size. An upstream or downstream movement of the ICS will not affect the reported data by more than 5–10%, if that.

Example 6: How will Tables 13, 14 and 15 assist in the design of an ICS?

1. Table 13 can be used regardless of the type of ICS selected. It gives the percentage of the total normal load (provided the structure is situated normal to the flowlines) at each measuring point. Since the structure was physically divided at the gap opening, the percentage of the total load taken by the U.S. and Canadian sections can also be found in Table 13. The U.S. section contained bars 1–4, while the Canadian portion had the remainder (5–11). A range in the average data can be extracted from Table 13.

2. Table 14 reflects the maximum percentage of the normal load taken at any one time at a particular measuring bar during one of the 112 transits. The maximum value has been highlighted. These data reflect some of the localized ice interaction phenomena very near the gap opening as a result of the ship passages. The data in Table 14 can be used with a floating ice control structure concept but not directly if a rigid structure is planned.

3. Tables 14 and 15 can be used if a floating ice control structure is considered. The position of the measuring bars can be assumed to be the end points of the individual floating sections, as they were in the model. An individual floating section might be as long as 120 to 190 m composed of smaller floating elements such as timbers or pontoons to retain the ice.

Both Tables 14 and 15 are measures of the extreme loads taken at any one point. This percentage can be compared in Table 13 to the average value measured for that measuring bar. The maximum value is generally two to three times the mean value for all bars.

Table 15 is slightly different than Table 14. The data contained in Table 15 are the ratio of maximum loads to the mean load at each position for both x and y directions using urea-doped ice. These data were abstracted from the dynamic force measurements *during* ship transits through the ICS and ice field. The ratios, except for the two end bars and a y direction on bar 3, are consistent with the values one would calculate by considering the data in Table 13 and 14. There are exceptions where the ratio is close to four, but generally the peak load to average load ratio is 2 to 3.

4. The design of a rigid structure to retain the ice at Port Huron would be based on the crushing strength of the ice; this load of 1380 to 2760 kN/m (200–400 lbf/in.^{2}) far exceeds the loading considered in this study using fragmented ice floes contained by a floating structure.

APPENDIX B. SUGGESTED ADDITIONAL STUDIES

The following section discusses areas where additional data collection is necessary to substantiate some findings in the physical model section. Also, areas are suggested where more research is needed to verify some of the assumptions in the wind stress analysis.

Physical model

The calibration of the physical model for ice-covered conditions requires knowledge of the shear stress exerted by the water to the underside of the ice sheet. Since only 10 measurements were available, additional data need to be gathered to verify the shear stress values obtained in February 1979. The decay in the shear stress as one goes farther into the lake would shed light on the assumptions used in the analysis of the influence of the portions of the lake outside the study area that could contribute load to an ice control structure.

To minimize any doubt about the open water calibration, another drogue study for a lower discharge (i.e. < 180,000 cfs) should be undertaken. More drogue lines, including additional lines closer to the two shorelines, should be used.

Winter conditions

The available data on ice movement into the St. Clair River are probably the most comprehensive ever taken to date at one site. To fully understand the ice processes at Port Huron, the following observations and measurements would provide the necessary backup information for the work already completed on ice arching and for evaluating potential environmental effects: 1) limits of the ice arch location, 2) shoreline ice pileup documentation, 3) shoreline profiles of the bed, 4) meteorological data near the site, 5) in-situ ice stress measurements, and 6) critical pressure determinations for ice deformation.

1. The ice arch location throughout the entire ice season would help verify the wind stress modeling work. Determining the ice conditions that lead to stabilizing a series of ice arches, particularly if ship traffic is occurring, would require an almost daily observation by air and close coordination of ship movements.

2. The shoreline ice pileup occurs now without a structure in place. Thus, existing ice pileups and windrows need to be documented in case severe ice conditions arise with an ice boom in place. Physical measurements of these pileups and their distribution over distance and time are needed. The distribution of these events can be mapped for aerial observations or photographic documentation. The physical measurements can be conducted by ground surveys with the proper ice augers, but a remote-sensing radar device may offer more flexibility and greater coverage. CRREL personnel have conducted one set of shore pileup measurements at Port Huron and Sarnia with the impulse radar. It appears from the initial playback of data that the technique of data collection is very critical, as height, speed and possibly the grounded ice are important in gathering reliable data. The radar method looks promising but data collection techniques need to be refined. Processing the data and interpreting the output will require field verification.

3. The shoreline bed profiles will establish the baseline data on the processes taking place over a winter season, as well as during the entire season. The ice pileup conditions probably disrupt the bed conditions, but how much and how frequently are not known. To answer these questions would require ground surveys prior to and following the ice season at several cross sections with tight vertical and horizontal control at each section. One midwinter observation might be necessary if ice conditions are very erratic. Both shorelines would need to be observed and a good set of low-level vertical photographs taken every two years to quantify any noticeable shoreline retreat over a 5- to 10-mile segment.

4. The measurement of in-situ ice stress and how it correlates with the prevailing wind direction and speed is a link to verify portions of the modeling concept. The details of how to make these measurements and where to make them should be worked out.

55

5. Determination of the critical pressure that initiates the ice cover to deform is needed. As mentioned in the wind stress modeling section this critical stress needs to be determined for ice ridging, rafting and shore pileup conditions. A laboratory study in a large refrigerated basin with an instrumented towing carriage and side walls instrumented to determine the total force balance would be necessary.

APPENDIX C. DERIVATION OF ICE DISCHARGE FREQUENCY ANALYSIS

Ice discharge in square kilometers per vessel transit through the ICS opening could vary from zero to some upper boundary value. Theoretically, the upper boundary value could be unrestrained, i.e. infinite. From the data range one could automatically eliminate a normal distribution function. Since the raw data exhibited a definite right skewness some form of an exponential function is suggested. Hydrologists frequently use the two-parameter gamma frequency distribution function for data analysis of extreme events: flood flows, rainfall, etc.

Due to the noticeable right-skewness in the data and the universal acceptance of the gamma distribution in statistical hydrology, it was assumed to be a reasonable distribution for fitting the data. The two-parameter gamma function is also called the Pearson Type III, and tables are found in most hydrology texts dealing with the use of tables for the incomplete gamma function based on frequency factors.

The 2-parameter gamma functions has the following distribution:

$$f(y) = \frac{1}{\beta^\alpha \, \Gamma(\alpha)} \; y^{\alpha-1} \; e^{-y/\beta} \qquad \begin{array}{l} \beta > 0 \\ \alpha > 0 \end{array}$$

where y = random variable ice discharge value
β = scaling parameter of y
α = shape parameter
Γ = usual gamma function.

The estimation of parameters α and β was evaluated by two methods. The maximum likelihood estimator (MLE) technique advanced by Thom (1957) was found to be superior over the method of moments and used in this analysis. The MLE for the gamma function is

$$\alpha = \frac{1 + 4/3 \left(\ln \overline{Y} - \frac{1}{n} \Sigma \ln y \right)}{4 \left(\ln \overline{Y} - \frac{1}{N} \Sigma \ln Y \right)}$$

where $\beta = \overline{Y}/\alpha$
$\overline{Y}$ = mean value
N = number of observations

The method of moment estimation for α is $\overline{Y}^2/S_y^2$, where S_y^2 is the variance of the y variable and β is calculated in the same manner.

The integral of the gamma probability density function yields the incomplete gamma function,

$$P(\alpha, \beta; \hat{Y}) = \int_0^{\hat{Y}} \frac{y^{\alpha-1} \, e^{-y/\beta}}{\beta^\alpha \, \Gamma(\alpha)} \, dy$$

where $\hat{Y}$ is the value of y at the upper limit of the integration. Defining $t = y/\beta$; $\beta dt = dy$ and changing the variables to functions of t yields

$$P(\alpha, \hat{Y}/\beta) = \int_0^{\hat{Y}/\beta} \frac{e^{-t} \, t^{a-1}}{\Gamma(\alpha)} \, dt$$

with further simplification to

$$P(\alpha, \dot{Y}/\beta) = \frac{1}{\Gamma(\alpha)} \int_0^{\dot{Y}/\beta} e^{-t} t^{\alpha-1} dt,$$

and

$$P(\alpha, \dot{Y}/\beta) = \frac{1}{\Gamma(\alpha)} \gamma(\alpha, \dot{Y}/\beta).$$

The chi-square distribution is also related to the incomplete gamma function where

$$P(\alpha, \dot{Y}/\beta) \simeq P(\chi^2 | \nu) \simeq \frac{1}{\Gamma(\alpha)} \gamma(\alpha, \dot{Y}/\beta)$$

$$\chi^2 = 2\dot{Y}/\beta$$

$$\nu = 2\alpha$$

and since $P(\chi^2 | \nu)$ can be approximated by a series expansion for small values of α

$$P(\alpha, \dot{Y}/\beta) \simeq \frac{1}{\Gamma(2\hat{\alpha}/\beta)} \sum_{n=0}^{\infty} \frac{(-1)^n (\dot{Y}/\beta)^{\alpha+n}}{n!(\alpha+n)}$$

The evaluation of the series was performed by factoring the recurrence interval until the absolute difference between two successive computations was less than 0.0001. Stability problems did occur with large values of α (>20) and when the area under the density function approached 0.9999. Also, a uniform data set was encountered where $\alpha \sim 35$; the series could not handle this alpha value.

The gamma function $\Gamma(x)$ for $0 < x < 1$, was also evaluated from a series expansion. The form was a polynomial approximation

$$\Gamma(x+1) = x! = 1 + a_1 x + a_2 x^2 + a_3 x^3 + a_4 x^4 + a_5 x^5$$

with $a_1 = -0.5748646$
$\quad a_2 = 0.9512363$
$\quad a_3 = -0.6998588$
$\quad a_4 = 0.4245549$
$\quad a_5 = -0.1010678$

The values of the gamma function for $n > 1$ were computed using the recurrence relation

$$\Gamma(n+z) = (n-1+z)(n-2+z)\dots(1+z)\,\Gamma(1+z)$$

where $\Gamma(1+z)$ is computed from the previous polynomial approximation for values less than 1. Hand calculations for these quantities are unthinkable; consequently a computer program for the Hewlett-Packard 9845B was written to evaluate the above series and values of the probabilities at the desired levels.

The ultimate goal was to determine the values of ice discharge per vessel transit at the various levels of exceedance. The ice discharge data were separated into two categories of vessel direction and ice type.

The computed values of means, standard deviations, skew coefficients, etc., can be found in Tables 10 and 11. The method of moments estimation was evaluated and the discharge values were generally close to those computed by the MLE method. All exceedance level discharge values reflect the MLE technique.

A straightforward method to use is the "frequency factor" approach when the data are already tabulated. This is obtained through a mathematical exercise of the term $Y_\gamma = \beta_\gamma$ and one arrives at

$$Y_\gamma = \dot{Y} + S_\gamma^2 K$$

where Y_γ = values of ice discharge at exceedance level $\gamma (T_\gamma)$

$\dot{Y}$ = mean ice discharge

S_γ^2 = variance of ice discharge

K = frequency factor = $\dfrac{t_\gamma - \alpha}{\alpha}$ = $f(T_\gamma, C_s)$

C_s = sample skew coefficient.

Tables of K values for the Pearson Type III function can be found in most recent hydrology texts. To find K, the skew coefficient, and probability levels are needed. The arithmetic skew coefficient for all data is found in the tables.

There are several data bases that contained zero ice discharge for vessel transits. The statistical quantities were computed for the non-zero events in the data base and then adjusted according to the relation

$$P_A\left(\alpha, \frac{\dot{Y}}{\beta}\right) = P_1 + S_1\ [P(\alpha, \dot{Y}/\beta)]$$

where $P_A(\dot{Y}/\beta)$ = adjusted probability for a value $< \dot{Y}/\beta$

$P_1 = \dfrac{n_0}{N}$

$S_1 = 1 - \dfrac{n_0}{N}$

n_0 = number of event with zero ice discharge

N = total number of ice discharge data points including zeros.

The mathematical functions for the incomplete gamma function were obtained from the U.S. Dept. of Commerce (1970).

59

A facsimile catalog card in Library of Congress MARC
format is reproduced below.